# Laser Measurements and Stochastic Simulations of Turbulent Reacting Flows

Sheridan C. Johnston, Robert W. Dibble, Robert W. Schefer,
William T. Ashurst, and Wolfgang Kollmann
*Sandia National Laboratories, Livermore, California*

## Introduction

ALTHOUGH nearly all combustion of fossil fuel is accompanied by turbulent fluid flow, the quantitative prediction of turbulent reacting flows remains in a highly evolutionary stage.[1-4] The development of models for turbulent combustion has proved to be difficult due to our limited understanding of turbulence and its complex interaction with flame chemistry and combustion thermodynamics. Recent evidence indicates that the use of submodels based on isothermal or nonreacting turbulent flows may not be valid in reacting flows.[5-7] Thus, there exists a critical need for well-conceived experiments that provide fundamental quantitative as well as qualitative data to be used to develop a more comprehensive understanding of turbulent combustion. Such data are of paramount importance in the development, testing, and improving of turbulent reacting flow models.

The discussion included herein is intended to give the reader a sampling of the state-of-the-art in both experimental and modeling approaches to the analysis of turbulent reacting flows, but it is not intended to be an exhaustive review of the field. Furthermore, it deals with the fundamental aspects of turbulent combustion and thus includes only occasional reference to more practical applications in boilers, furnaces, or internal combustion engines.

In the first part of the paper, the application of laser-based diagnostics to turbulent reacting flows is discussed. Included in this discussion are laser velocimetry,[5-7] Rayleigh,[7-9] and Raman[10,11] scattering, and the simultaneous application of these diagnostic techniques.[12] In the second part, three different approaches to the modeling of turbulent reacting flows are discussed. These include the moment, the probability density function, and the vortex dynamics approaches. Model predictions of some portions of the experimental results described in the first part of the paper are discussed, as are predictions of other chemically reacting flows documented in the literature. Most of these comparisons between modeling predictions and experimental measurements have not been previously published.

## Laser Probes for Turbulent Flames

Laser probes in turbulent environments are particularly useful, since they provide a means for obtaining information that is both spatially and temporally resolved. Spatial resolution is achieved through detection of signals generated at the focus of a single laser beam or from multiple laser beams whose foci are coincident. Temporal resolution for scalar measurements is most often achieved through the use of pulsed laser sources whose pulse duration is in the nanosecond to several microseconds range. In most applications, this information is obtained without disturbing the processes being interrogated.

The initial applications of laser light scattering to gas-phase systems were in chemically inert environments. Techniques were developed to measure gas velocity using scattering from particles,[13-15] total gas density using scattering from molecules,[16] and gas composition and temperature using spon-

**Sheridan C. Johnston is supervisor of the Combustion Physics Division of the Combustion Research Facility. The research activities of this group consist of turbulent reacting flows, combustion applications of laser diagnostics, soot formation, and propellant combustion. He has a Ph.D. in mechanical engineering from the University of California at Davis and graduate degrees from the von Kármán Institute for Fluid Dynamics and Rensselaer Polytechnic Institute.**

**Robert W. Dibble is a member of the technical staff in the Combustion Physics Division of the Combustion Research Facility. His research interests include spectroscopy, chemical kinetics, and turbulent reacting flows. He has a Ph.D. in chemical engineering from the University of Wisconsin at Madison.**

**Robert W. Schefer is a technical staff member in the Combustion Physics Division of the Combustion Research Facility. His research interests include turbulent nonreacting and reacting flows, the application of laser diagnostics to combustion systems, and catalytic combustion. He has a Ph.D. in mechanical engineering from the University of California at Berkeley.**

**William T. Ashurst is a member of the technical staff in the Combustion Research Facility. Past research activities include aerodynamics, numerical fluid dynamics, molecular dynamics simulation of fluid transport, and discrete vortex dynamics simulation of turbulent flow. He has a Ph.D. in applied science from the University of California at Davis.**

**Wolfgang Kollmann is Professor of Mechanical Engineering at the University of California at Davis and a visiting scientist at the Combustion Research Facility. Prior to this, he was a faculty member at the von Kármán Institute for Fluid Dynamics. His research interests are centered around modeling turbulent flows and, more recently, turbulent flames. He has a doctorate from the Technische Hochschule at Aachen, FRG.**

Presented as Paper 84-0543 at the AIAA 22nd Aerospace Sciences Meeting, Reno, NV, Jan. 9-12, 1984; received Dec. 13, 1984; revision received Feb. 15, 1985. 

taneous Raman spectroscopy.[17-19] Later, these diagnostics were applied to gas-phase systems undergoing chemical reaction.[20,21] These combustion applications initially concentrated on laminar flow systems, which provided a convenient and stable environment for diagnostic development, but as the fundamental underlying physics of the diagnostics were more fully understood, applications to turbulent combustion emerged.[22-25]

By proper design of the experiment, it is possible to resolve the structure of turbulent flames with a spatial resolution down to the Kolmogorov microscale and with a temporal resolution for which chemical reactions are frozen in time. Such measurements are achievable either at a single point using a focused laser beam, along a line,[26,27] or in a plane using multidimensional imaging techniques that are capable of providing a planar snapshot of a large region of a turbulent flame.[28,29] Further development of planar imaging techniques to higher framing rates should provide the potential for quantitative detection of large-scale structures in a Lagrangian reference frame.

It is convenient to categorize the underlying scattering processes into ones that are elastic, with no change in wavelength, and into ones that are inelastic, with a molecule-specific shift in scattered-light wavelength. Elastic processes include Mie scattering from particles (which forms the basis for laser velocimetry) and Rayleigh scattering and resonant fluorescence from molecules. Inelastic processes include linear effects such as spontaneous Raman scattering and laser-induced fluorescence, as well as nonlinear effects such as coherent anti-Stokes Raman spectroscopy (CARS) and inverse Raman spectroscopy.[30] Only linear processes will be considered here. For a comprehensive description of laser velocimetry (LV), the reader is referred to the many articles and reviews in the literature.[13-15]

### Rayleigh Scattering

Few examples exist of the application and development of laser Rayleigh scattering for combustion research, primarily because the technique lacks molecular specificity and is susceptible to interferences from elastic scattering from particles and surfaces. This has occurred in spite of the fact that Rayleigh cross sections are 1000 times greater than rotational-vibrational Raman cross sections. However, through a judicious design of the experiment, laser Rayleigh scattering can be used to measure temperature (or density) at a rate, and hence a frequency response, higher than any other present day laser-based technique.[9]

In Ref. 9, the expression for Rayleigh scattering intensity is shown to have the form

$$I_s = CI\Omega\ell\frac{PA_0}{RT}\left(\frac{d\sigma}{d\Omega}\right)_{eff} = \frac{K}{T}\left(\frac{d\sigma}{d\Omega}\right)_{eff} \quad (1)$$

where $C$ is calibration constant of the collection optics, $I$ the incident laser intensity, $\Omega$ the solid angle of the collection optics, $\ell$ the length of the laser beam segment imaged onto the detector, $P$ the pressure, $A_0$ the Avogadro number, $R$ the universal gas constant, and $T$ the absolute temperature. The effective Rayleigh differential cross section of the gas mixture is given by the sum of the mole-fraction-weighted cross sections $(d\sigma_i/d\Omega)$,

$$\left(\frac{d\sigma}{d\Omega}\right)_{eff} = \sum_i X_i\left(\frac{d\sigma_i}{d\Omega}\right) \quad (2)$$

Since laser intensity is assumed to be constant (a good assumption in nonabsorbing, nonsooting gas-phase combustion), variations in the Rayleigh scattering intensity can result from temperature or species concentration variations, or both. The unambiguous interpretation of the Rayleigh-scattered intensity requires that experiments be designed according to the principles described subsequently.

Unless stated to the contrary, the measurements described below were made in the Sandia Turbulent Diffusion Flame Facility, an induced-draft wind tunnel with an axisymmetric fuel jet located at the upstream end of a test section (Fig. 1). The fully windowed test section has a 30 $cm^2$ cross section and is 200 cm long. The fuel nozzle inside diameter $D$ is 0.53 cm. The bulk velocity of the fuel mixture (0.22 mole fraction of argon in hydrogen) is 154 m/s and the coflowing air stream velocity is 8.5 m/s. The jet Reynolds number is 24,000.

*Case 1. Constant Rayleigh Cross Section: Temperature Measurement*

In this case, variations in the Rayleigh scattering intensity are attributed to variations in gas temperature. Through a judicious selection of fuel composition, the variation in the Rayleigh cross section for fuel, air, and products can be reduced to less than 2%, even for initially nonpremixed reactants.[9] Probability distributions of temperature for a premixed methane-air flame measured using Rayleigh scattering at several axial locations along the flame centerline are shown in Fig. 2. Similar measurements have been made by other workers.[31-33] Temperature distributions obtained in a fully turbulent nonpremixed flame are shown in Fig. 3, where $x/D$ is the nondimensionalized distance downstream from the nozzle exit and $y/D$ the nondimensionalized radial distance measured from the nozzle centerline.

*Case 2. Constant Temperature: Mole Fraction Measurement*

In this case, variations in the Rayleigh scattering intensity are due to variations in the effective Rayleigh differential cross section, i.e., to variations in the mole fraction.

The feasibility of making time-resolved measurements of the dispersion of a turbulent methane jet into air was demonstrated by Graham and co-workers.[16] Quantitative measurements of the dispersion of a propane jet into air were made by Dyer[34] as a preliminary test of a diagnostic that was later used to map fuel-air distribution in an internal combustion (IC) engine combustion simulator.[35]

*Case 3. Constant $\sigma_i/m_i$: Density Measurement*

It is possible to measure density using Rayleigh scattering when the fuel, oxidizer, and products each have the same

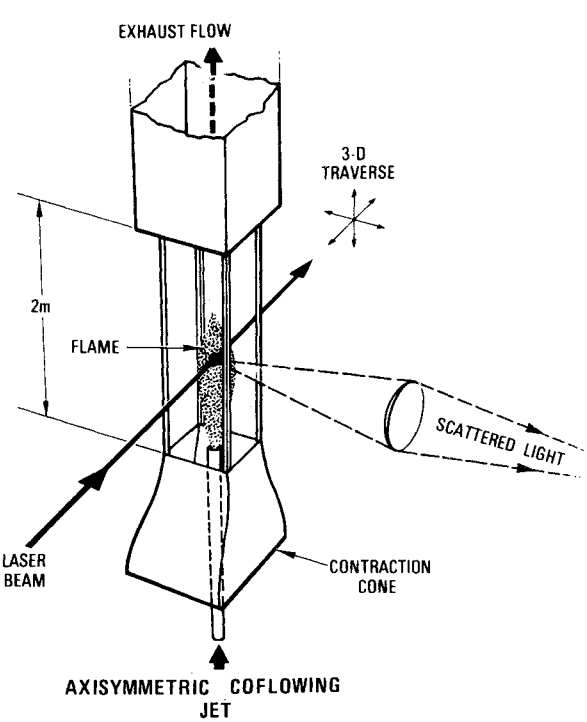


**Fig. 1 Schematic of the Sandia Turbulent Diffusion Flame Facility. Optical access is provided for a variety of laser diagnostics, which remain fixed spatially while the entire combustion tunnel can be translated in three orthogonal directions.**

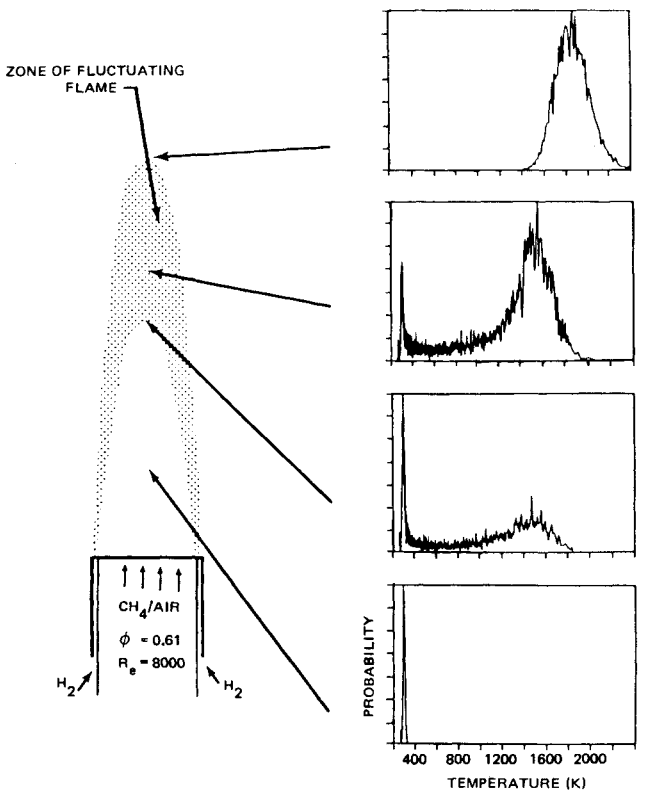


**Fig. 2 Laser Rayleigh thermometry in a turbulent premixed flame. Probability distribution of temperature at indicated locations in the flame.**

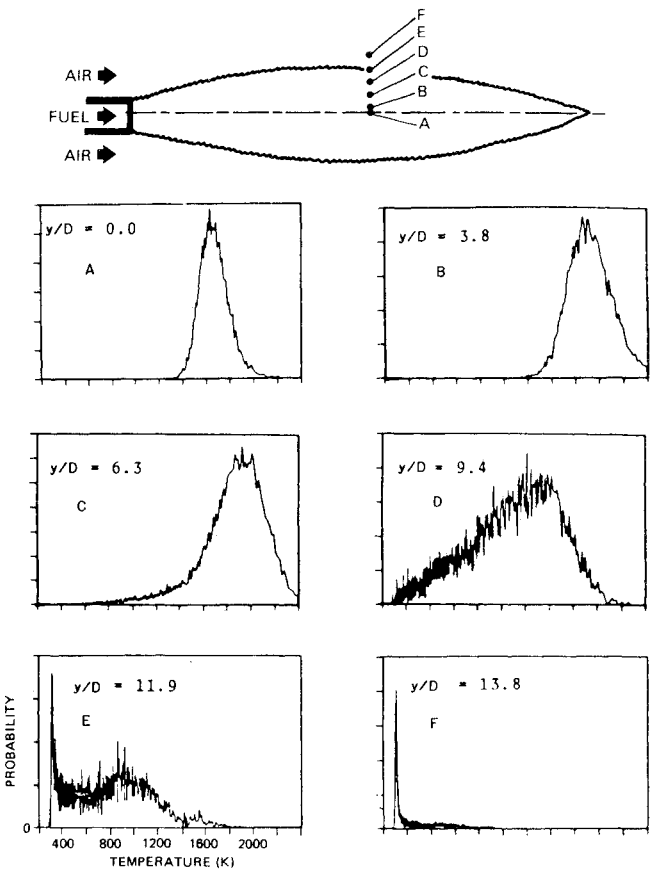


**Fig. 3 Laser Rayleigh thermometry in a turbulent jet diffusion flame. Probability distributions of temperature at axial position $x/D = 65$ and various radial positions $y/D = 0.0$, 3.8, 6.3, 9.4, 11.9, 13.8.**

value of $\sigma_i/m_i$, where $\sigma_i$ is a shorthand notation for the differential cross section and $m_i$ the molecular weight of either the fuel, oxidizer, or products.

By making use of the ideal gas equation of state, Eq. (1) can be written as

$$I_s = C_1 \sum_i n_i m_i \left(\frac{\sigma_i}{m_i}\right) \tag{3}$$

When all $\sigma_i/m_i$ are equal, Eq. (3) becomes

$$I = C_1 C_2 \sum n_i m_i = \rho C_1 C_2 \tag{4}$$

where $n_i$ is the number density of the $i$th species.

Most common fuels have values of $\sigma_i/m_i$ greater than that of air; therefore, either argon or helium, which have values of $\sigma_i/m_i$ less than air, can be added to the fuel to achieve the desired properties of the combustible mixture and combustion products. For example, for a fuel mixture of 22% argon in hydrogen, the values of $\sigma_i/m_i$ for the fuel, air, and products are equal to within 2.9%.

Probability distributions of gas density $\rho$ normalized by air density $\rho_0$ in a turbulent nonpremixed flame are shown in Fig. 4 and the mean axial and radial density variations across the jet flame in Fig. 5. Also shown in Fig. 5 are model calculations of gas density, which will be discussed later.

*Case 4: Varying Temperature and Rayleigh Cross Section*

In this case, additional information is required, which could be obtained from another diagnostic or from a mathematical model. Smith[36] used extensive computations of a laminar hydrogen diffusion flame to predict the species distribution throughout the flame. With this information, the temperature could be inferred from the Rayleigh scattering intensity.

**Raman Scattering**

The use of spontaneous Raman scattering for thermometry and concentration measurement has been reviewed by several authors.[19,37,38] Although both pure and rotational[18,39] and and rotational-vibrational[40] transitions can be used for temperature and concentration measurements, rotational-vibrational (Q-branch) spectra are generally preferred for flame applications because of the relative freedom from spectral overlap of different molecular species.

For the purpose of this paper, the salient feature of spontaneous Raman spectroscopy is that the integrated charge $Q_i$ from a photomultiplier tube is linearly related to laser energy $Q_\ell$ and species concentration $[N_i]$ as follows:

$$Q_i = k_i Q_\ell [N_i] f_i(T) \tag{5}$$

The proportionality constant $k_i$ is dependent on the vibrational Raman cross section, wavelength, and optical collection efficiency and is ultimately determined by calibration. Typically, calibration is accomplished using rotational-vibrational Raman scattering from gas samples at room temperature and pressure. The bandwidth factor $f_i(T)$ accounts for the temperature-dependent distribution of molecules in their allowed quantum states. Also convolved into $f_i(T)$ are the spectral location, shape, and bandwidth of the spectrometer and the bandwidth of the laser. Calculation of $f_i(T)$ is possible for diatomic molecules such as $N_2$, $O_2$, and $H_2$; however, the calculation is less reliable for triatomics such as $H_2O$. Thus, after calibration, a measurement of species concentration will require that laser pulse energy, Raman signal, and temperature be measured simultaneously.

Smith[41] and Eckbreth[42] have shown that the need for a temperature measurement can be reduced or eliminated by careful attention to the parameters affecting the bandwidth factor. This can also be achieved by specifying the temperature as a function of, for example, the nitrogen

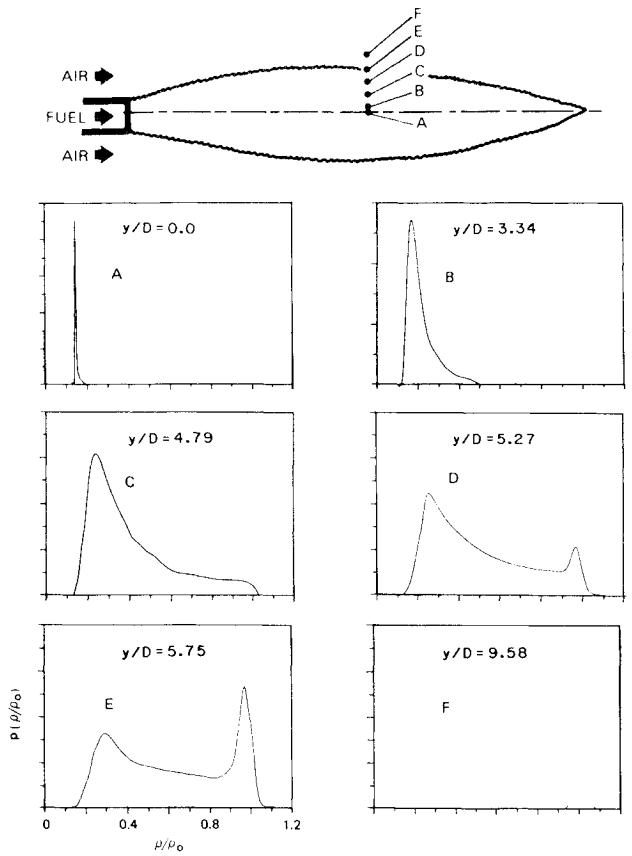


**Fig. 4 Probability density distributions of gas using Rayleigh scattering at an axial location of $x/D = 50$ in a turbulent nonpremixed flame.**

concentration:

$$f_i(T) = f_{N_2}(T[N_2])$$

In a nonpremixed flame, a unique relationship between the nitrogen concentration and the temperature can be determined when it can be assumed that: 1) the chemical kinetics are fast relative to the rate of mixing (large Damköhler number); 2) the mixing is dominated by turbulence and, hence, all species and enthalpy are transported at the same rate (unity Lewis number); and 3) the flow is adiabatic. These assumptions have been examined and shown to be valid for the jet flame discussed herein.[12]

One result of making the above assumptions is that all of the concentrations and temperatures can be related to a single conserved scalar, as shown by Bilger[43] and Mitchell.[44] The conserved scalar $\zeta$ is an algrebraic combination of reactive scalers, e.g., fuel and product concentrations such that $\zeta$ is independent of the progress of chemical reaction: During a chemical reaction, the numerical value of $\zeta$ is conserved. Changes in $\zeta$ are then due only to turbulent and molecular transport. An example of such a conserved scalar is the local instantaneous concentration of atoms originating from the nozzle fluid divided by the total atom concentration. In the nozzle, $\zeta$ has the value of unity and, in the freestream air, zero.

The relationship between $\zeta$ and other scalars is illustrated in Fig. 6, where equilibrium relationships were computed using the procedure of Reynolds.[45] The monotonic relationship between $[N_2]$ and $\zeta$ is the route through which $\zeta$ is determined from the measurement of the nitrogen Raman signal. A major advantage of this method is that the nitrogen concentration and its Raman signal are greater than those of all other species until the mixture is substantially fuel rich, $\zeta > 0.59$. In actual practice, the $[N_2]$—$\zeta$ relationship was used only when the mixture fraction was fuel lean, a condition that existed for most of the data. When the mixture was fuel rich, ($[O_2] < [H_2]$), $\zeta$ was

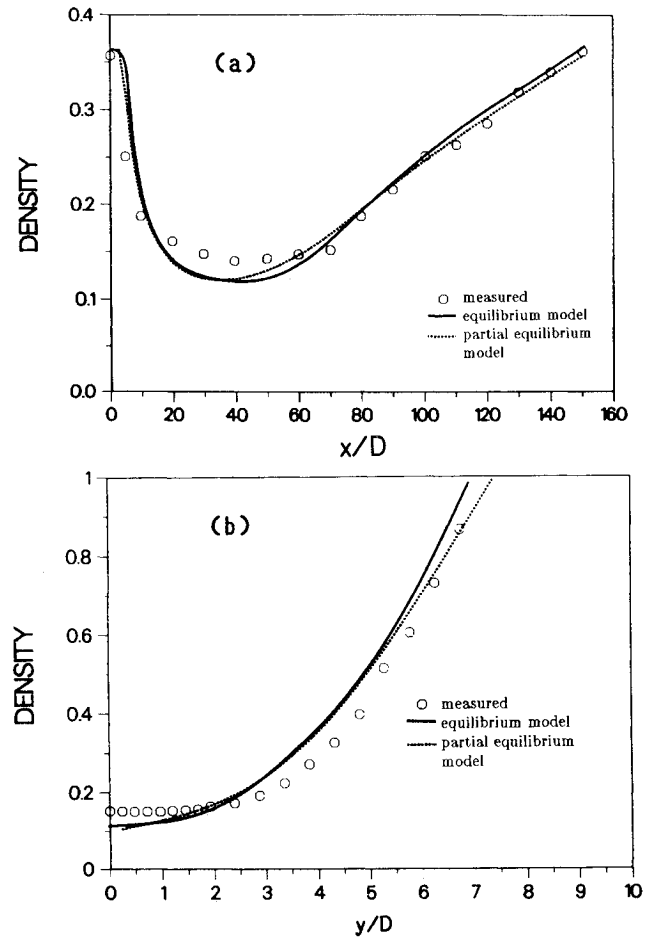


**Fig. 5 Predicted variations of mean density $\rho/\rho_0$ are compared with Rayleigh scattering measurements: a) centerline, b) radial. Model predictions indicate that, for this hydrogen-argon-air flame, chemical kinetic rates are fast enough that an equilibrium chemistry model is indistinguishable from a model that includes finite-rate chemical kinetics.**

determined from the $[H_2]$—$\zeta$ relationship (Fig. 6). Hydrogen concentrations were determined from Eq. (5) in a manner entirely analogous to that for the nitrogen concentration.

Atomic mixture fraction measurements are shown in Fig. 7, for which the mean and rms fluctuation of $\zeta$ are depicted. From these atomic mixture fraction results, total gas density (Fig. 8) and temperature (Fig. 9) can be obtained using the data reduction procedure described above. Concentration profiles of nitrogen and oxygen are shown in Fig. 10 and hydrogen and water vapor profiles in Fig. 11. Figures 6-11 were taken from Ref. 12. The experimental setup used to obtain these data will be described later.

### Simultaneous Velocity-Scalar Measurements

Turbulent flows have transport rates several orders of magnitude greater than the molecular transport rates occurring in nonturbulent flows. These higher rates are a consequence of the correlations between fluctuating components of velocity ($u'$, $v'$, and $w'$) and of correlations between velocity and fluctuating scalar state variables such as temperature $T'$, density $\rho'$, or species concentration. Most turbulent flow models include a submodel for such correlations. Ideally, the submodel should be tested by direct comparison with correlation measurements. Although a variety of submodels have been proposed, none has been tested in this manner because of the paucity of correlation measurements. Instead, it has been necessary to resort to comparisons of overall model predictions with measured mean values. Unfortunately, this comparison is an insensitive measure of the accuracy of the

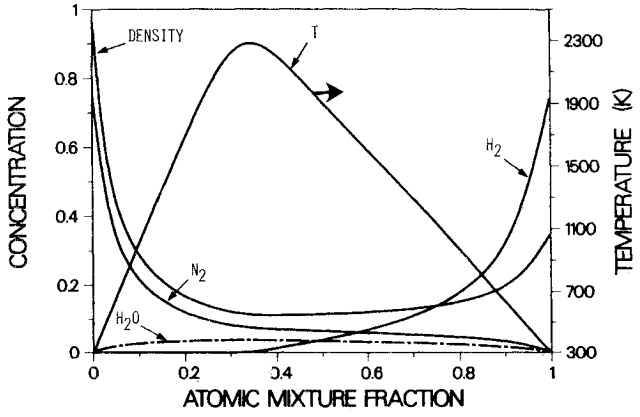


**Fig. 6 Equilibrium value of the scalars $[N_2]$, $[H_2O]$, $[H_2]$, $\rho/\rho_0$, and $T$ are plotted against the atomic mixture fraction, $\zeta$. Note: $\zeta_{stoichiometric} = 0.32$ and concentrations are relative to air at NPT.**

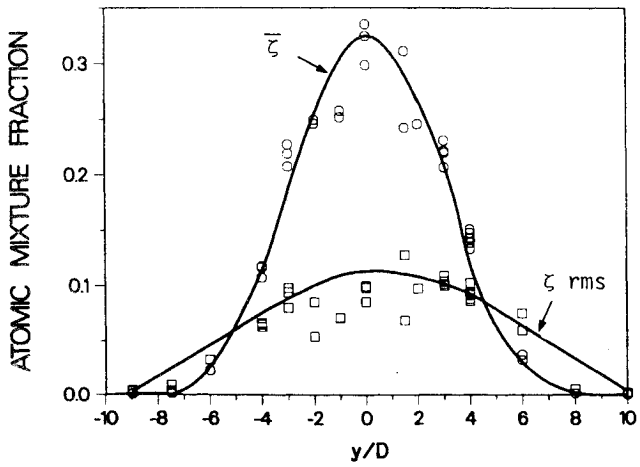


**Fig. 7 Measured mean and fluctuation rms of atomic mixture fraction $\zeta$ plotted as a function of radius at $x/D = 50$.**

correlation submodels. What is needed are direct and unambiguous measurements of these correlations.

Simultaneous LV-Rayleigh scattering was used to obtain density-velocity correlations and simultaneous LV-Raman scattering was employed to determine conserved scalar-velocity correlations, both in a turbulent nonpremixed flame.[7,12] The density-velocity correlations $\rho'u'$ and $\rho'v'$ are important because they appear explicitly in the time-averaged Navier-Stokes equations. These terms represent axial and radial turbulent mass fluxes, respectively. The conserved scalar-velocity correlation is of particular importance to the modeling of turbulent nonpremixed reacting flows.

In addition to density-velocity correlations, simultaneous LV-Rayleigh scattering has been used to obtain density-velocity point probability distributions, which are important in recent modeling approaches such as those of Pope.[77]

*LV-Rayleigh Scattering*

The combined LV-laser Rayleigh scattering apparatus (Fig. 12) has been described elsewhere.[7] Exact simultaneity in measuring velocity and density is not possible with this technique, since the Rayleigh signal is invalid when an LV seed particle is present in the laser probe volume. However, in the work described herein, the minimum nonsimultaneity time interval, 40 $\mu$s, was short enough compared to the characteristic time of the turbulent flow that the measurements are considered to be essentially simultaneous.

1) *Density-Velocity Correlations $\overline{\rho'u'}$ and $\overline{\rho'v'}$.* In the variable-density flows considered here, the turbulent mass flux

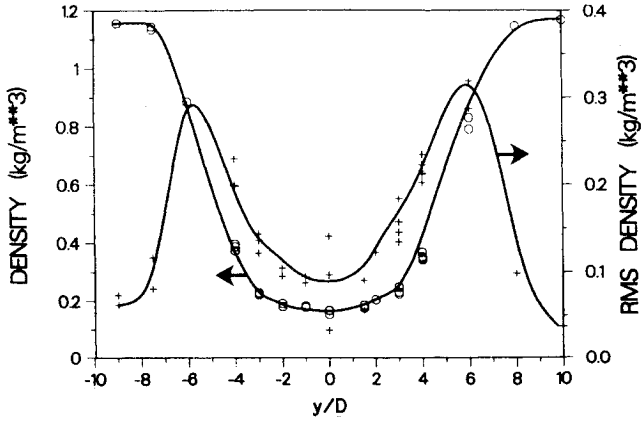


**Fig. 8 Measured mean and fluctuation rms of density plotted as a function of radius at $x/D = 50$.**

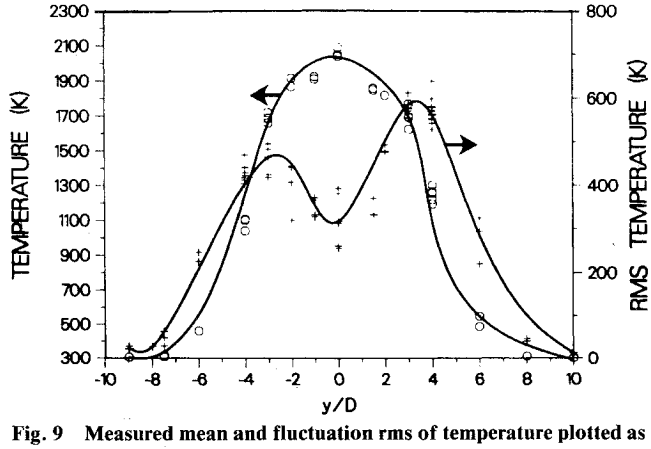


**Fig. 9 Measured mean and fluctuation rms of temperature plotted as a function of radius at $x/D = 50$.**

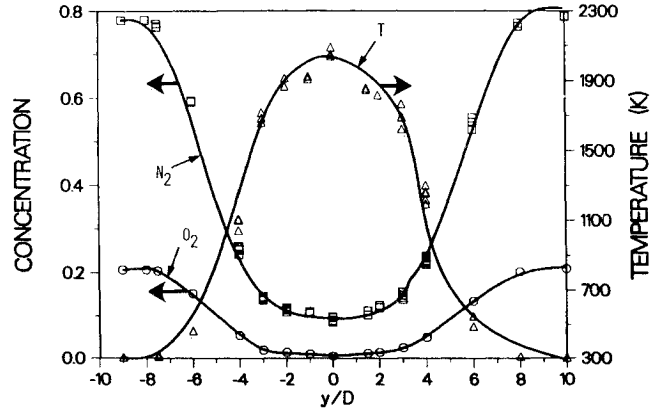


**Fig. 10 Profiles of $[N_2]$, $[O_2]$, and temperature plotted as functions of radius at $x/D = 50$. The concentrations are relative to air at NPT. Lines are smooth fits through the data.**

vector plays an important role in the development of turbulent shear flows by controlling the influence of mean pressure gradients on the transport of momentum and scalars. A detailed analysis[46,47] of the equations for the density-velocity correlations shows that the correlations are produced by the gradients of velocity and density and that the pressure correlation provides the destructive mechanism and modifies the production terms.

Values of the correlations $\overline{\rho'u'}$ and $\overline{\rho'v'}$ measured in the flame are shown in Figs. 13 and 14. Combined measurements

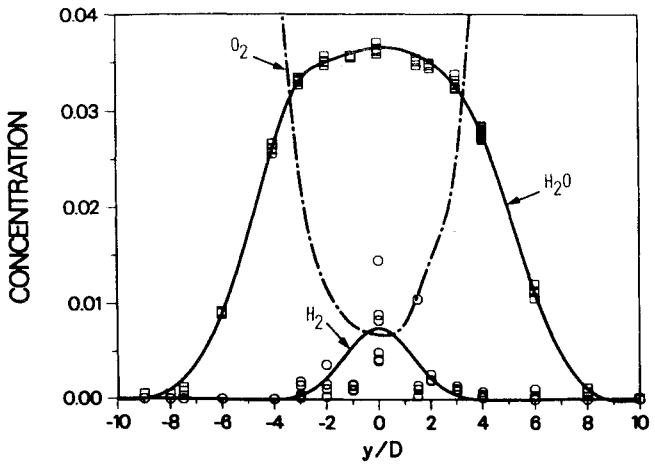


**Fig. 11 Profiles of $[O_2]$, $[H_2]$, and $[H_2O]$ plotted as a function of radius at $x/D=50$. The concentrations are relative to air at NPT. Lines are smooth fits through the data.**

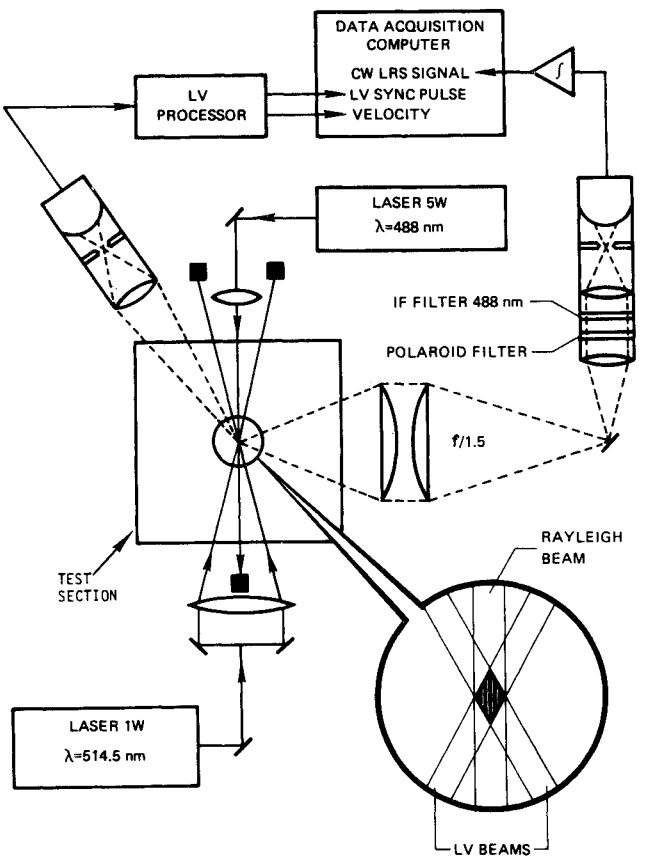


**Fig. 12 Schematic diagram of combined Rayleigh scattering-laser velocimeter apparatus.**

such as these can be used to assess submodels of the density-velocity correlation as it appears in the Reynolds- or Favre-averaged momentum equation.[47-50] The density-velocity correlation is often modeled in flames using gradient-diffusion relations such as

$$\overline{\rho' u'} = -D_T \frac{\partial \bar{\rho}}{\partial x} \text{ and } \overline{\rho' v'} = -D_T \frac{\partial \bar{\rho}}{\partial y} \qquad (6a,b)$$

where $D_T$ is a non-negative turbulent diffusivity.

The data of Fig. 13 are direct experimental evidence of countergradient diffusion in nonpremixed flames. A major

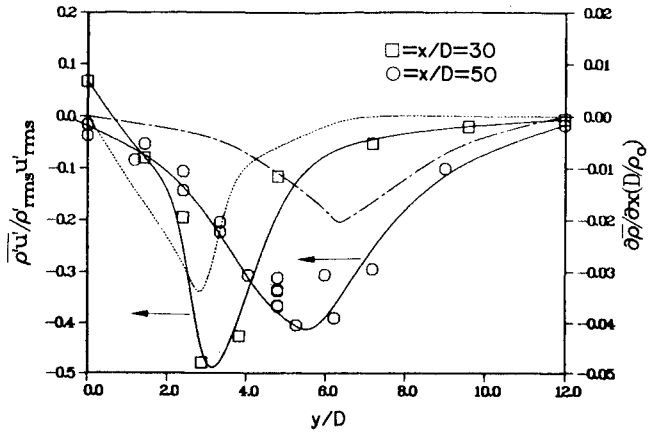


**Fig. 13 Radial profiles of axial density-velocity correlations $\rho' u'/(\rho'_{rms} u'_{rms})$ and normalized axial density gradient $\partial\bar{\rho}/\partial x (D/\rho_0)$ [..., $\partial\bar{\rho}/\partial x(D/\rho_0)$ at $x/D=30$; — at $x/D=50$].**

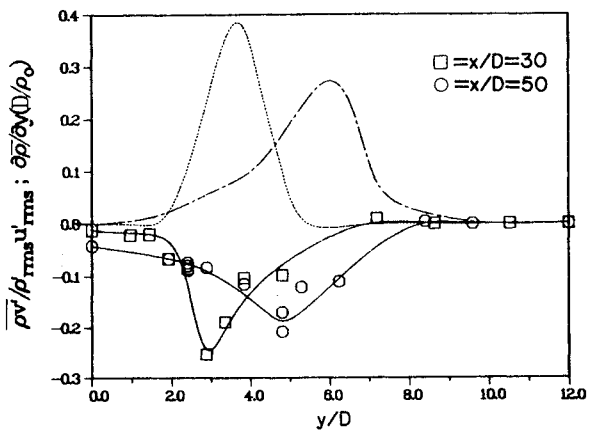


**Fig. 14 Radial profiles of radial density-velocity correlations and normalized radial density gradient [....$\partial\bar{\rho}/\partial y(D/\rho_0)$ at $x/D=30$; — at $x/D=50$].**

conclusion to be drawn from Fig. 13 is that the correlations $\overline{\rho' u'}$ are negative where the measured axial density gradients $\partial\bar{\rho}/\partial x$ also are negative. This result implies that Eq. (6a) cannot be physically descriptive because a negative diffusivity would be required. However, results obtained at other locations in the flame indicate that regions are also present where the axial density gradient and the correlation $\overline{\rho' u'}$ have opposite signs. For these regions, a gradient diffusion appears to be a reasonable modeling assumption. Furthermore, the measured radial mass flux $\overline{\rho' v'}$ is consistent with a gradient diffusion relation Eq. (6b) throughout the flowfield, as seen by the data of Fig. 14.

Further analysis of these data[7] has shown that both the axial and radial density-velocity correlations are dominated by the radial gradients, which are approximately 10 times larger than the axial gradients. From these and similar results, it is concluded that a closure model for the correlations should at least include both the radial and axial gradients. More likely, it will be necessary to replace Eqs. (6) with a second-order closure model. Then the local flux is no longer directly related to the local mean gradient, but also depends on the history of the fluid element, which is more consistent with the actual "nonlocal" nature of turbulence.

2) *Density-Velocity Joint Probability Distributions.* Joint probability distributions of axial velocity and normalized density at $x/D=50$ are shown in Fig. 15. The distribution at $y/D=5.75$ is characterized by a relatively narrow Gaussian distribution in velocity, particularly at higher densities. At

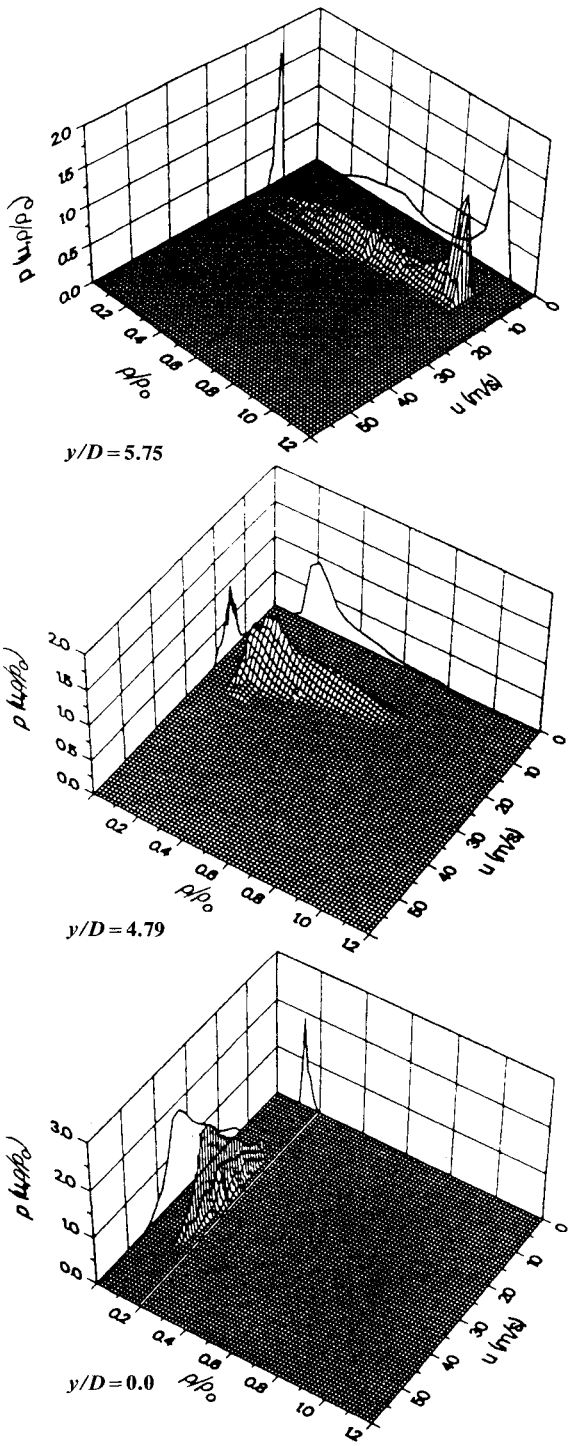


Figure. 15 Joint probability density distributions of axial velocity and density in a turbulent nonpremixed flame at an axial location of $x/D = 50$.

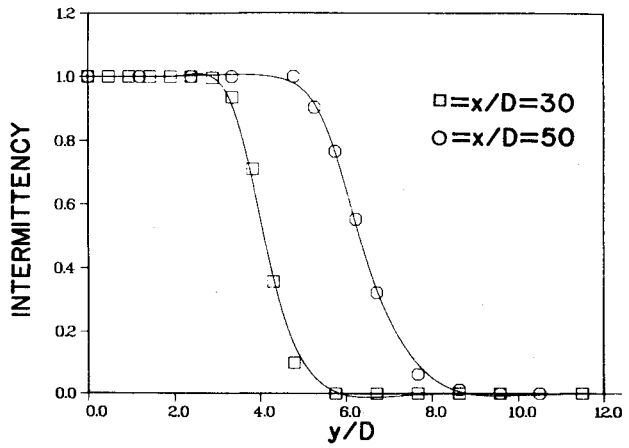


Fig. 16 Intermittency factor as a function of normalized radial distance.

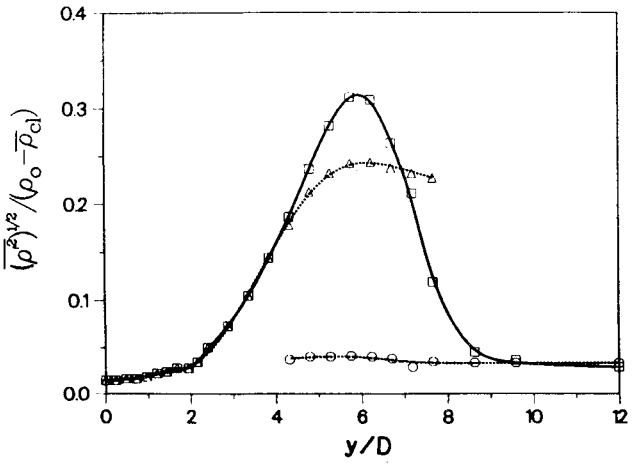


Fig. 17 Radial profiles of conventional and conditional gas density fluctuations for a turbulent nonpremixed flame at an axial location of $x/D = 50$ (□ conventionally averaged density fluctuations; △ conditionally averaged density fluctuations in turbulent fluid; ○ conditionally averaged density fluctuations in nonturbulent fluid; $\rho_0$ is air density and $\bar{\rho}_{cl}$ is centerline density).

lower densities, an increase in the turbulent fluctuation level is indicated by some skewing in the velocity distribution toward the higher velocities. Contributions to the probability density distribution from both the air and the mixture of fuel and combustion products are apparent. Bilger[51] has suggested that continued entrainment of coflowing air distorts the Gaussian distribution to which the turbulent product gas density would otherwise tend. This leads to a lack of a well-defined separation between the reactant and product gas distributions.

At $y/D = 4.79$, the primary density contribution to the joint probability distribution is due to low-density product or fuel gases with very little high-density air present. The velocity distribution, while still Gaussian, has broadened considerably, particularly for the lower-density gases, and is slightly skewed toward the higher velocities. At the centerline ($y/D = 0$), the gas density is narrowly distributed about the stoichiometric equilibrium density and the velocity distribution is well represented by a Gaussian that is slightly skewed toward the lower velocities.

Under the demonstrated conditions of fast chemical kinetic rates, the reacting flow considered here can exist in any one of three states: 1) pure air, 2) pure fuel, or 3) a mixture of fuel and products or a mixture of air and products. Significant density differences exist between these different fluid compositions. These density differences have been used to discriminate between the different fluid-dynamical zones in the turbulent diffusion flame to obtain information about intermittency.

Intermittency is defined as the probability that a given flow is turbulent at a given point and time. The proper measure of whether or not the flow is turbulent involves the variance of the vorticity fluctuations (enstrophy), a quantity that is experimentally difficult to measure. As a result, a scalar measurement is often used to distinguish between fluid that is turbulent and fluid that is irrotational. In the particular case described here, the Schmidt number (a relative measure of the diffusion of vorticity to the diffusion of mass) is unity. Thus, it is argued that when the measured density is below some frac-

tion of the irrotational air density, gas mixing has occurred. It is further argued that, because the value of the Schmidt number is unity, vorticity has also diffused to that mixture element and the fluid element is therefore turbulent.

For the reacting flow measurements discussed here, the intermittency factor $\gamma$ is defined as the fraction of time that the instantaneous gas density $\rho$ is less than the freestream air density $\rho_0$. For densities above a certain threshold value, $\gamma$ is set equal to zero (corresponding to freestream air or nonturbulent fluid) and, for densities less than the threshold value, the fluid is considered as turbulent ($\gamma = 1$). The method of Bilger et al.[52] was used to determine a threshold density corresponding to freestream air and resulted in a normalized threshold density $\bar{\rho}/\rho_0$ of 0.95 for the results presented in Fig. 16, where the ensemble-averaged intermittency is shown as a function of normalized radial distance.

It is significant to the turbulent transport in jet flames that, at both axial locations in the present study, a region exists near the centerline in which the intermittency is unity. Only in a relatively well-defined mixing region for which $\gamma$ is between 0 and 1 are both high-density air and lower-density fuel and combustion products present. These results are considerably different from those obtained in liquids (much higher Schmidt number and much lower Reynolds number) in which nonturbulent fluid was found on the jet centerline.[27]

Experimental techniques based on conditional sampling have been developed to better understand the nature of intermittency through the characterization of the turbulent and nonturbulent fluid states.[53-56] These studies have been carried out largely in nonreacting flows. Fluctuating density data can be averaged in at least two different ways: 1) conventional averaging in which no distinction is made between the turbulent and the nonturbulent parcels of fluid; and 2) conditional averaging in which intermittency is used to conditionally sample the density, depending on whether it is in a turbulent or nonturbulent region. Radial profiles of the conditionally averaged, fluctuating density are compared with the conventionally averaged profiles in Fig. 17. Conditionally averaged density fluctuations in the turbulent fluid increase less rapidly in the inner region of the jet than the conventionally averaged values, but are higher in the outer part of the flow. Fluctuation levels in the nonturbulent fluid increase only slightly across the mixing zone. Based on these results, it might be expected that a turbulence model accounting for the difference in turbulent and nonturbulent zone properties has a much firmer physical basis and is potentially more accurate for reacting flows where the chemical reaction rates are strongly dependent on such local flow properties as temperature.

*LV-Raman Scattering*

In this work, the scalar-velocity correlations were made with a combined laser velocimeter-laser Raman scattering apparatus (Fig. 18) that has previously been described.[12] In brief, an LV event was used to trigger the pulsed laser, whereupon the species concentration and temperature could be calculated from the pulsed-laser Raman scattering. Since the time delay between the LV event and the laser pulse is small (40 $\mu$s) relative to the characteristic time scale of the turbulent flow, the measurements are essentially simultaneous.

The Raman optical detection system was designed such that, at the exit plane of the spectrometer (Fig. 18), five photomultiplier tubes were positioned to receive the Stokes-shifted vibrational Raman scattered light from $N_2$, $O_2$, $H_2$, $H_2O$, and the anti-Stokes vibrational Raman scattering from $N_2$. In addition, the elastically scattered (Rayleigh and Mie) laser light was also measured. These measurements, along with simultaneous velocity measurements from the LV optical apparatus, were used to determine the velocity-scalar correlation.

A typical experimental run produced a data matrix with 160 rows (laser shots) and 8 columns: axial velocity $u$, $Q_{N_2}$, $Q_{O_2}$, $Q_{H_2}$, $Q_{H_2O}$, $Q_{N_2-AS}$, $Q_{\text{Rayleigh}}$, and $Q_{\text{laser}}$. This data matrix was reduced to a $160 \times 2$ matrix of velocity and conserved scalar ($u$-$\zeta$) pairs by use of the data reduction method described above and shown in Fig. 6.

Components of a typical $u$-$\zeta$ matrix are plotted in Fig. 19, which is the scatter diagram of axial velocity and atomic mixture fraction. Each point represents a single LV-laser Raman event. Scatter in the data is due to random fluctuations and not to experimental error, the standard deviation of which is typically less than 6%. From the $u$-$\zeta$ matrix, combined with

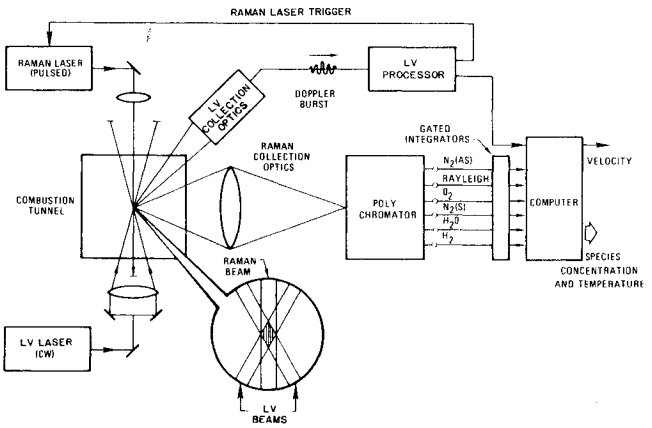


**Fig. 18 Schematic showing the principle components of the combined LV-laser Raman scattering system.**

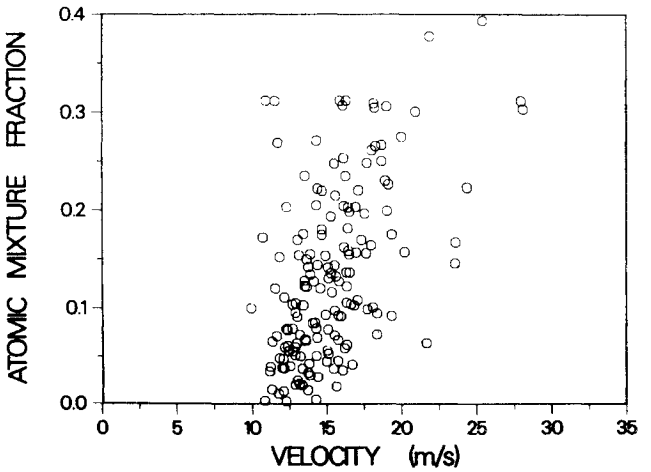


**Fig. 19 Joint probability plot of velocity and $\zeta$ constructed from 160 LV-Raman events collected at $y/D = 4$ and $x/D = 50$.**

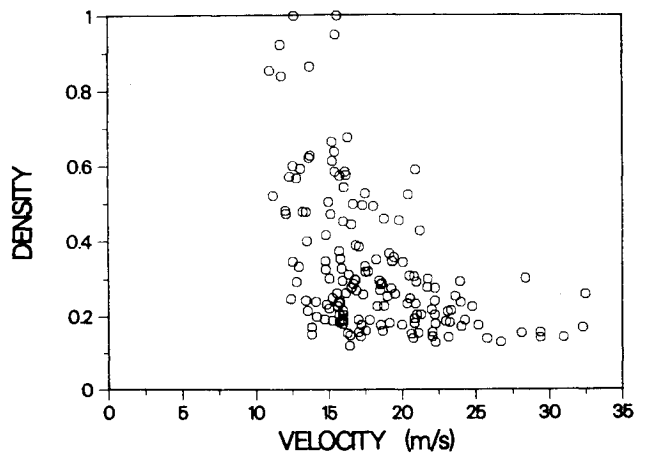


**Fig. 20 Joint probability plot of velocity and density $\rho/\rho_0$ constructed from the 160 LV-Raman events.**

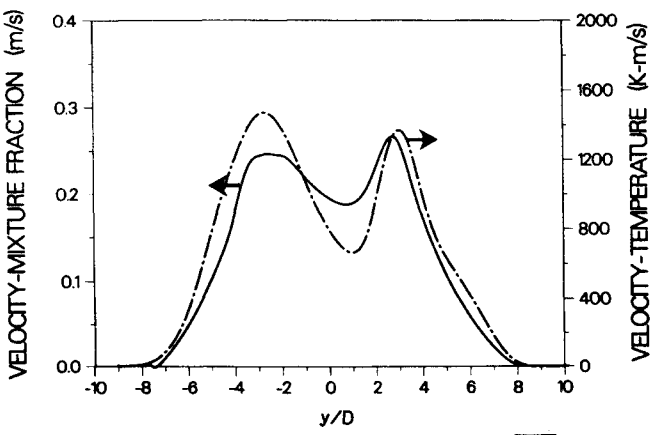


**Fig. 21 Measured velocity-temperature correlation $\overline{u'T'}$ (broken line) and the velocity-mixture fraction correlation $\overline{u'\zeta'}$ (solid line) plotted as a function of radius at $x/D = 50$.**

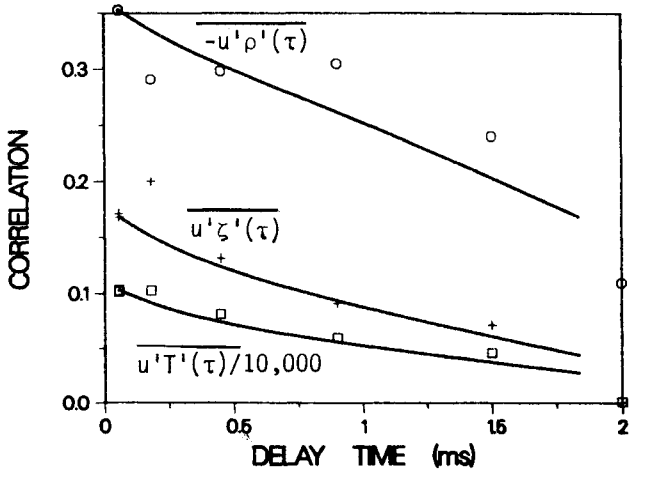


**Fig. 22 Measured temporal velocity-scalar correlation for density $\overline{u'\rho'}(\tau)$, atomic mixture fraction $\overline{u'\zeta'}(\tau)$ and temperature $\overline{u'T'}(\tau)$ plotted as a function of delay time at $x/D = 50$, $y/D = 4$.**

the equilibrium table described previously, all of the subsequent results and figures are generated. The $u$-$\zeta$ matrix plotted in Fig. 19 has been transformed to a $u$-$\rho$ matrix and is plotted in Fig. 20.

Velocity-Scalar Correlations: Correlations of fluctuating axial velocity $u'$ with $\zeta'$ and $T'$ are presented in Fig. 21. The close agreement between $\overline{u'\zeta'}$ and $\overline{u'T'}$ is a consequence of the axial measurement station, $x/D = 50$, being just beyond the flame tip. At this location, the flow is characterized primarily by the mixing of hot combustion products with the surrounding air.

Figure 22 presents the temporal velocity-scalar correlations for density, temperature, and atomic mixture fraction. While caution is needed in drawing conclusions from so few data points, it is instructive to form the product of the correlation half-life ($\sim 1.5$ ms) and the local mean velocity (15 m/s) to arrive at a macrolength scale of 2 cm. This length is one-third the flame diameter at this location and is consistent with the often used order-of-magnitude assumption that the length scale of a turbulent jet is on the order of its diameter.[57]

## Modeling

Numerical modeling predictions of turbulent reacting flows can be approached in several different ways, which can be loosely grouped into two categories: 1) those that extend constant-density turbulence models and develop new constants in order to obtain agreement with experiment or 2) those that simulate time-dependent mixing and reacting flow and strive to define new turbulence models. Each approach requires a different set of assumptions and individual models yield different kinds of information about the reacting flow considered.

Classical turbulence models (approach 1) approximate turbulent velocities with mean and fluctuating components and develop transport models for the time-averaged effects of turbulence. Included in this category are both moment and probability density function (pdf) models. These methods have been quite successful in developing engineering tools that are calibrated with known experiments. The lack of fundamental physics is indicated by the need to change the model constants for different flow geometries, e.g., planar vs round jets. However, from a fundamental viewpoint, the meaning of concepts such as mean velocity may be questioned. For example, turbulent wall shear stress occurs in bursts in which the stress exceeds the time-averaged value by as much as 60 times. Thus, the actual time-dependent stress is highly intermittant and not simply related to the time-averaged velocity gradient often assumed in these models. However, if only time-averaged information is required, then such models are adequate and valuable. But, if detailed time-dependent mixing is required, for example, to describe temperature-sensitive chemical reactions, then the time-averaged models can be very misleading.

Certainly, there have been successful efforts with the first approach and one may wonder if the second approach needs to be taken at all. Considering the advancements in computer hardware, the second approach is not completely unreasonable and thus deserves some effort because, if it is successful, the payoff will be tremendous. For example, a computer calculation that resolves all important time and length scales in turbulent combustion will provide information that is currently inaccessible experimentally, but yet is vital to improving our understanding of reacting turbulent flows. Currently, direct computation of the effects of intermittent flow structures on chemical reaction is feasible in two dimensions. Predictions of pressure fluctuation in three-dimensional turbulence would allow verification of the modeled pressure-strain terms in the turbulent transport equations.

Such time-dependent calculations will most likely remain too expensive to serve as an engineering parametric study tool and will never simulate all length scales in the flowfields that occur in most practical applications. Thus, this second approach must focus on statistical properties of small fluid volumes. But, once calibrated by time-dependent data, a computer model resolving all important length and time scales will be a valuable "laboratory" for theoretical development.

### Moment Approach: Two-Equation and Second-Order Closure Models

Moment models involve the classical moment approach and generate the least amount of information in terms of first- and second-order moments. They require many closure assumptions of varying levels of arbitrariness in which higher-order moments are modeled by analogy to constant-density, nonreacting flows in terms of lower-order moments. Concern has been expressed that the chemical reaction sufficiently alters the turbulent flows to make this approach suspect. However, these models are applicable to many problems and do not require excessive computing power.

Turbulent reacting flows with large heat releases (and therefore strong density fluctuations) require closure assumptions or simplifications that can be organized into three groups: thermochemical, turbulence, and coupling models. The three groups will be discussed in turn.

#### *Thermochemical Model*

Successful application of this model depends crucially on the chemical composition of the fuel. Gaseous fuels such as hydrogen and hydrocarbons react with air as the oxidizer in a

complex system of reactions involving many steps and a large number of components. For higher hydrocarbons, the reaction mechanisms are not known completely, making accurate calculations impossible even for laminar flames.

Fortunately, consideration of detailed reaction mechanisms for the prediction of mean flow quantities (velocity, pressure, density, temperature) is not necessary and a simple (global) one-step reaction suffices.[58] Finite-rate chemistry is required, however, for the prediction of pollutant formation, unburned fuel concentration, and flame ignition and extinction.[59]

1) *Diffusion Flames.* Diffusion flames burning hydrogen or lower-order hydrocarbons have been modeled using an infinitely fast, one-step reaction mechanism.[60] Under these conditions, it is possible to establish a local relation between the density, temperature, and composition to a conserved scalar (mixture fraction). These relations are highly nonlinear and a coupling model (pdf) is required to calculate the mean thermodynamic state. Such a model couples the pdf of the mixture fraction into the analysis. A description of this model will be given in a later section. For the prediction of nonequilibrium effects, the one-step mechanism is inadequate and additional scalar variables, which are not conserved, have to be included.[61,62]

2) *Premixed Flames.* The conserved scalar approach does not work for premixed flames (because the conserved scalar, mixture fraction is constant in this case) and mean reaction rates must be calculated. Most work in this area has been based on a global reaction step.[63,64] The most advanced model was developed by Bray et al.[64] and describes the reaction in terms of a single-reaction progress variable. The pdf of this variable is then appropriately represented by spikes from the completely burned and unburned fluid and a continuous part from the reacting fluid. For large Damköhler and Reynolds numbers, the coefficient of the continuous part is small. The shape can be inferred from a laminar flamelet description of the reaction zone.

*Turbulence Model*

Most models use Favre-averaged statistics to obtain a compact description of the influence of density fluctuations. In general, the Favre-averaged variable $\tilde{\phi}$ is defined as $\tilde{\phi} \equiv \overline{\rho\phi}/\bar{\rho}$, where the bar represents a conventional time average and the tilde mass averaging. Fluctuations about the mass-averaged mean are denoted by a double prime, i.e., $\phi = \tilde{\phi} + \phi''$.

Two-equation turbulence models such as the $k$-$\epsilon$ model of Jones and Launder[65] have been applied to reacting flows[66,67] with some success. Second-order closures for reacting flows, however, are still in the developmental stage and the object of active research.[66,68,69] One such model[69] will be discussed in some detail here to highlight some of the difficulties encountered. This model is a preliminary form of the second-order closure model where all of the stress equations are included in the system, but the two scalar-flux equations are not yet included. The mean velocity satisfies

$$\bar{\rho}\partial_t \tilde{v}_\alpha + \bar{\rho}\tilde{v}_\beta \partial_\beta \tilde{v}_\alpha = -\partial_\beta(\bar{\rho}\widetilde{v_\alpha'' v_\beta''}) - \partial_\alpha \bar{p} \tag{7}$$

where viscous effects are neglected, $\bar{p}$ is the mean thermodynamic pressure, and Cartesian tensor notation is used (Greek subscripts). A closure assumption is not necessary. The Reynolds-stress components follow from

$$\begin{aligned}\bar{\rho}\partial_t \widetilde{v_\alpha'' v_\beta''} + \bar{\rho}\tilde{v}_\gamma \partial_\gamma \widetilde{v_\alpha'' v_\beta''} &= -\bar{\rho}\widetilde{v_\alpha'' v_\gamma''}\partial_\gamma \tilde{v}_\beta \\ &\quad - \bar{\rho}\widetilde{v_\beta'' v_\gamma''}\partial_\gamma \tilde{v}_\alpha + \partial_\gamma \mathcal{D}_{\alpha\beta\gamma} + Q^I_{\alpha\beta} \\ &\quad + Q^{II}_{\alpha\beta} - \overline{v_\alpha''}\partial_\beta \bar{p} - \overline{v_\beta''}\partial_\alpha \bar{p} - \tfrac{2}{3}\delta_{\alpha\beta}\bar{\rho}\epsilon\end{aligned} \tag{8}$$

where $\delta_{\alpha\beta}$ is the Kronecker delta.

The diffusive flux $\mathcal{D}_{\alpha\beta\gamma}$ is modeled according to Daly and Harlow[70] by

$$\mathcal{D}_{\alpha\beta\gamma} \simeq C_s \bar{\rho}(k/\epsilon)\widetilde{v_\gamma'' v_\delta''}\partial_\delta \widetilde{v_\alpha'' v_\beta''} \tag{9}$$

This form is considerably simpler (in particular, in axisymmetric coordinates[71]) than the model suggested by Hanjalic and Launder[73] and leads, in constant-density flows, to roughly the same results. For the zero trace part $Q^I_{\alpha\beta}$ of the pressure-strain rate correlation, the closure of Hanjalic and Launder is applied to density-weighted moments,

$$\begin{aligned}Q^I_{\alpha\beta} \simeq &-C_1\bar{\rho}\frac{\epsilon}{k}\left(\widetilde{v_\alpha'' v_\beta''} - \frac{2}{3}\delta_{\alpha\beta}k\right) - \frac{C_2+8}{11}\bar{\rho}\left(P_{\alpha\beta} - \frac{2}{3}\delta_{\alpha\beta}P\right) \\ &- \frac{8C_2-2}{11}\bar{\rho}\left(D_{\alpha\beta} - \frac{2}{3}\delta_{\alpha\beta}P\right) - \frac{30C_2-2}{55}\bar{\rho}k(\partial_\alpha \tilde{v}_\beta + \partial_\beta \tilde{v}_\alpha)\end{aligned} \tag{10}$$

where

$$k = \tfrac{1}{2}\widetilde{v_\alpha'' v_\alpha''}$$

$$P_{\alpha\beta} \equiv -\widetilde{v_\alpha'' v_\gamma''}\partial_\gamma \tilde{v}_\beta - \widetilde{v_\beta'' v_\gamma''}\partial_\gamma \tilde{v}_\alpha, P \equiv \tfrac{1}{2}P_{\alpha\alpha}$$

$$D_{\alpha\beta} \equiv -\widetilde{v_\alpha'' v_\gamma''}\partial_\beta \tilde{v}_\gamma - \widetilde{v_\beta'' v_\gamma''}\partial_\alpha \tilde{v}_\gamma$$

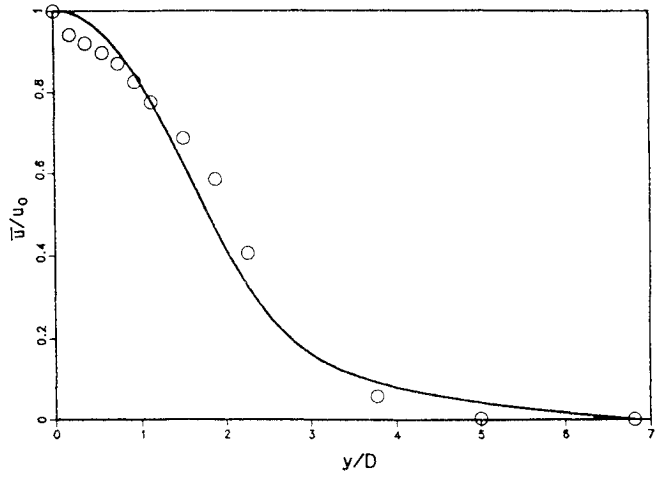


**Fig. 23 Radial variation of normalized mean velocity $\bar{u}/u_0$ at $x/D = 30$ for a turbulent diffusion flame (symbols: experiments of Driscoll et al.[7]).**

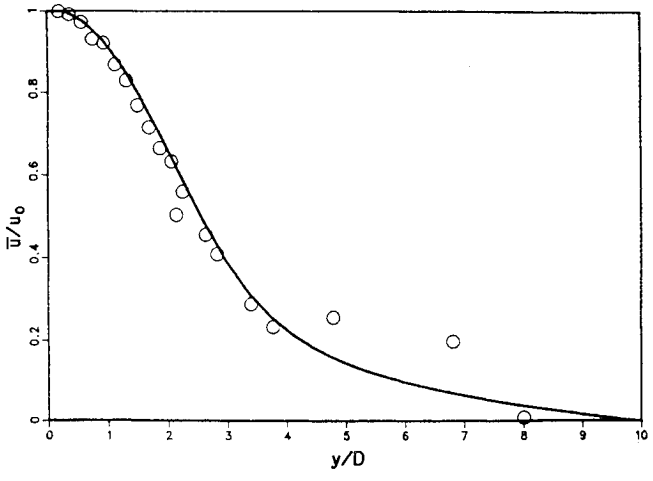


**Fig. 24 Radial variation of normalized mean velocity $\bar{u}/u_0$ at $x/D = 50$ (symbols as in Fig. 23).**

The model for part $Q_{\alpha\beta}^{II}$ of the pressure-strain correlation, which contains contributions due to the mixing and chemical heat release, presents great difficulty; thus, a first attempt is based on several considerations. The reactive part is determined by the location and movement of the instantaneous flame front, because only near the flame front does an expansion due to heat release take place. Since the fluctuations in the density occur only if the mixture fraction $f$ is below the stoichiometric value $f_{st}$, the correlation of the velocity and mixture fractions or density, together with the probability that the point considered is on the entrainment side ($f \leq f_{st}$) of the instantaneous flame front, determines the second part of the pressure-strain correlation. Thus, the model

$$\tfrac{2}{3}\delta_{\alpha\beta}\overline{\rho' D''} = Q_{\alpha\beta}^{II}$$

$$\simeq -C_{R1}\widetilde{v_\alpha'' v_\beta''}\cdot g^{1/2}\cdot(\widetilde{\rho' v_\gamma''})/\bar{\rho}\cdot\partial_\gamma[\bar{\rho}P(f_{st})] \quad \text{for } \alpha=\beta$$

$$\simeq 0 \quad \text{for } \alpha\neq\beta \qquad (11)$$

for normal stress components and no contribution to shear stress components is suggested. $P(f)$ denotes the probability density function of the mixture fraction. The mixing part can be neglected because it vanishes with the Reynolds number in pure mixing flows. Scales of length and time are determined by the rate of dissipation, which satisfies the following model equation:

$$\bar{\rho}\partial_t\epsilon+\bar{\rho}\tilde{v}_\alpha\partial_\alpha\epsilon=\partial_\alpha[C_\epsilon\bar{\rho}(k/\epsilon)\widetilde{v_\alpha'' v_\beta''}\partial_\beta\epsilon]$$

$$-C_{\epsilon1}\bar{\rho}(\epsilon/k)\widetilde{v_\alpha'' v_\beta''}\partial_\beta\tilde{v}_\alpha-C_{\epsilon2}\bar{\rho}(\epsilon^2/k)+P_R \qquad (12)$$

where $P_R$ contains the effect of the chemical heat release on the dissipation.This complex process is tentatively taken into account in a manner analogous to the corresponding term in Eq. (11) for the normal stresses,

$$P_R \simeq C_{R2}\epsilon\cdot g^{1/2}\cdot(\rho'\widetilde{v_\gamma''/\rho})\partial_\gamma[\bar{\rho}P(f_{st})] \qquad (13)$$

The statistical properties of the scalar variable (mixture fraction) are determined by its mean $\tilde{f}$ and its variance $g\equiv\widetilde{f''^2}$, plus the assumption that the pdf of $f$ is a beta function.[66] The mean value $\tilde{f}$ is the solution of

$$\bar{\rho}\partial_t\tilde{f}+\bar{\rho}\tilde{v}_\alpha\partial_\alpha\tilde{f}=\partial_\alpha[C_f\bar{\rho}(k/\epsilon)\widetilde{v_\alpha'' v_\beta''}\partial_\beta\tilde{f}] \qquad (14)$$

and the variance $g=\widetilde{f''^2}$ follows from

$$\bar{\rho}\partial_t g+\bar{\rho}\tilde{v}_\alpha\partial_\alpha g=\partial_\alpha[C_g\bar{\rho}(k/\epsilon)\widetilde{v_\alpha'' v_\beta''}\partial_\beta g]$$

$$+2C_f\bar{\rho}\frac{k}{\epsilon}\widetilde{v_\alpha'' v_\beta''}\partial_\beta\tilde{f}\partial_\alpha\tilde{f}-C_{g1}\bar{\rho}g\frac{\epsilon}{k}\left[1+\frac{1}{2}\frac{(\overline{\rho'^2})^{1/2}}{\bar{\rho}}\right] \qquad (15)$$

Exponents of the beta function are determined by the mean and variance. Thus, all expectations of local functions of the mixture fraction such as density, temperature, and composition[59] can be calculated by integration.

Application of the closure model to axisymmetric flow requires modification of two constants: $C_{\epsilon2}^{*}=1.95$ and for the shear stress component $\widetilde{u''v''}$, $C_1^{*}=2.5$. All the constants are summarized in Table 1. The values of $C_s$, $C_1$, $C_2$, $C_\epsilon$, $C_{\epsilon1}$, and $C_{\epsilon2}$, given in Table 1 were recommended by Launder and Morse[71].

**Table 1 Model constants**

| | | |
|---|---|---|
| $C_s=0.22$ | $C_{\epsilon1}=1.45$ | $C_f=0.15$ |
| $C_1=1.5$ | $C_{\epsilon2}=1.90$ | $C_g=0.17$ |
| $C_2=0.4$ | $C_{R1}=1.0$ | $C_{g1}=2.5$ |
| $C_\epsilon=0.15$ | $C_{R2}=0.5$ | |

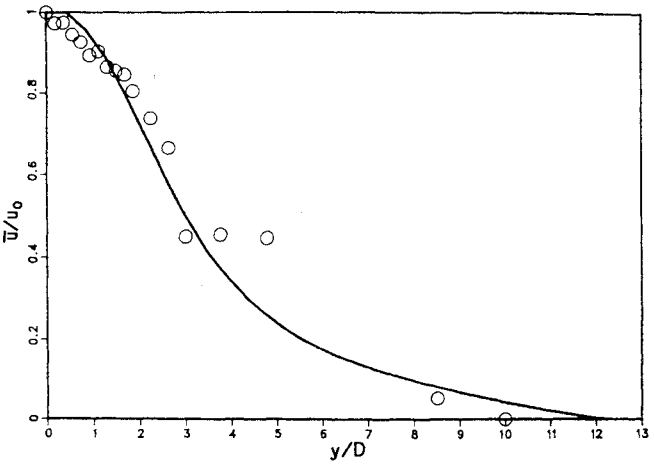


**Fig. 25 Radial variation of normalized mean velocity $\bar{u}/u_0$ at $x/D=70$ (symbols as in Fig. 23).**

*Coupling Model*

The local relations yielding density, temperature, and composition are functions of the conserved scalar (mixture fraction) and are highly nonlinear. It is therefore not possible to express the mean density or mean temperature in terms of the mean and variance of the mixture fraction. Thus, the pdf $P(f)$ of the scalar describing the instantaneous thermochemical state according to the model described above is required for the calculation (by integration) of mean temperature, density, and composition. Since moment models do not calculate the pdf, it must be constructed from the information provided by the model. The minimum information consists of the means and variances of the scalars.

For a single scalar, the beta function

$$P(f)=\frac{\Gamma(\alpha+\beta)}{\Gamma(\alpha)\Gamma(\beta)}f^{\alpha-1}(1-f)^{\beta-1} \qquad (16)$$

is an acceptable choice for $P(f)$. In Eq. (16), $\alpha$ and $\beta$ are the exponents of the beta function. However, this pdf does not represent all forms of $P(f)$ that have been observed experimentally.[74] Inclusion of the third moment[75,76] would improve the situation considerably, but it might then be preferable to solve the pdf transport equation directly instead of using an additional moment equation.[79]

*Moment Model Prediction: Turbulent Jet Flame*

The turbulent diffusion flame experiment of Driscoll et al.[7] offers an excellent test case, because of the relatively high Reynolds number (24,000), which is achieved using the addition of argon to the hydrogen fuel. Some representative results using the model described by Eqs. (7-16) are presented in Figs. 23-28 in the form of radial profiles at $x/D=30$, 50, and 70.

The mean normalized velocity

$$\bar{u}/u_0\equiv(\bar{u}-u_e)/(u_0-u_e)$$

in Figs. 23-25 shows good agreement with experimental data. In this notation, $u_0$ and $u_e$ are the mean velocity at the fuel jet exit and the average coflowing airstream velocity, respectively. Since the $y$ coordinate is normalized with the jet pipe diameter $D$ and not with the jet half-width, these figures show in addition that the spreading rate is correctly calculated. The normal

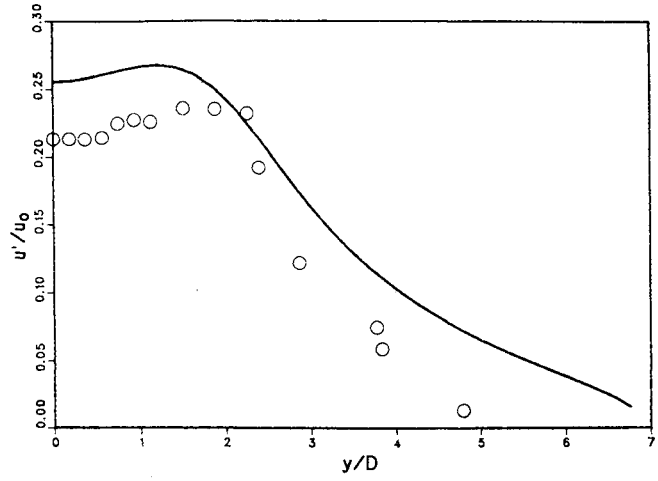


Fig. 26 Radial variation of normalized intensity of longitudinal velocity fluctuations $u'/u_0$ at $x/D=30$ (symbols as in Fig. 23).

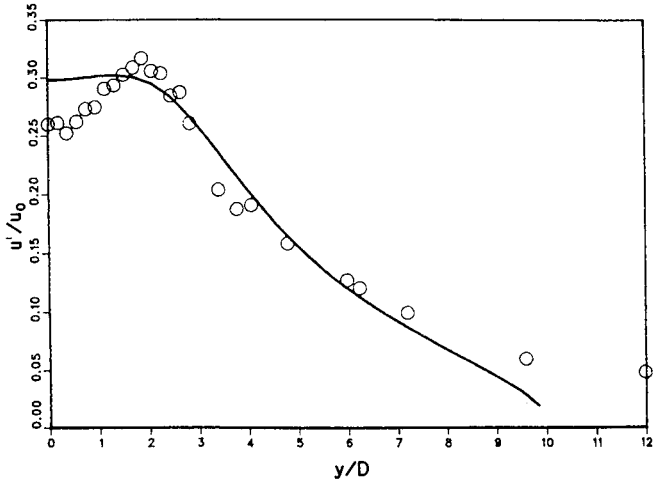


Fig. 27 Radial variation of normalized intensity of longitudinal velocity fluctuations $u'/u_0$ at $x/D=50$ (symbols as in Fig. 23).

stress profiles

$$u'/u_0 \equiv (\tilde{u''^2})^{1/2}/(u_0-u_e)$$

in Figs. 26 and 27 also show good agreement with the data. In Figs. 28, the shear stress

$$\overline{uv}/u_0^2 = \widetilde{u''v''}/(u_0-u_e)^2$$

is qualitatively similar to the profile for constant density, but is somewhat higher.

The mean density for $x/D=70$ in Fig. 29 shows good agreement with the experiments except in the outer part of the flame where the calculated profile is too low. Density fluctuations shown in Fig. 30 are too high in the outer part. This discrepancy can be explained by consideration of the beta function as the pdf. It clearly is not able to represent a pdf showing a relative maximum, as was found experimentally.[74] The beta function is U-shaped in the outer region, which necessarily leads to an overprediction of the density fluctuations.

#### Probability Density Function (pdf) Approach

Probability density function models allow exact (closed) representation of certain processes, such as finite-rate chemistry on turbulent diffusion, depending on the number of independent variables carried in the pdf. Thus, they yield more information about the flow and require fewer assumptions than moment models, but they also require more expensive solution procedures.

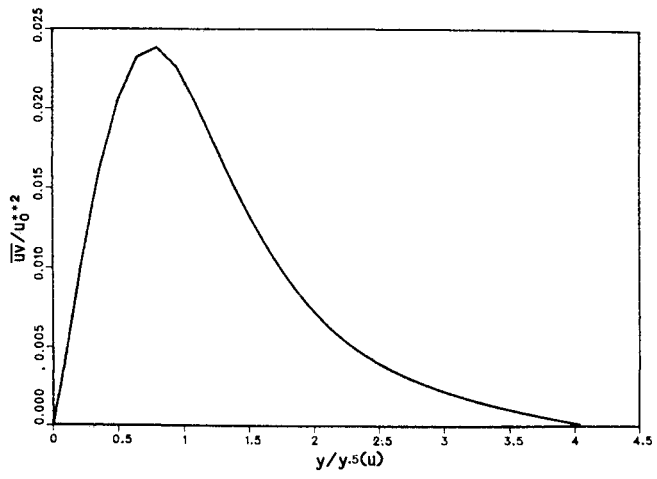


Fig. 28 Normalized shear stress $\overline{uv}/u_0^2$ at $x/D=70$ ($y$ normalized with velocity half-width).

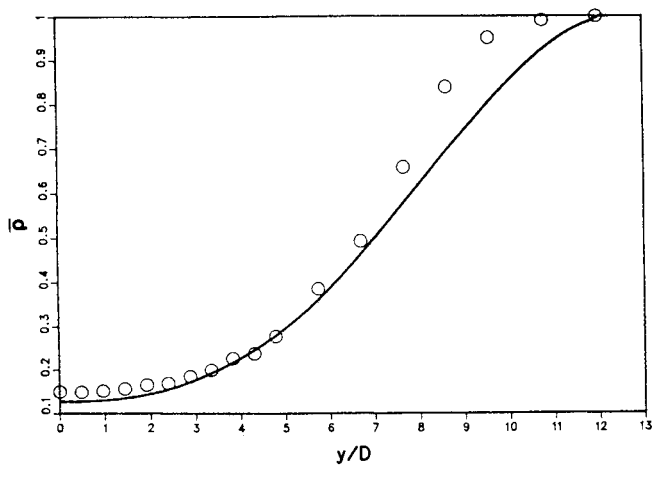


Fig. 29 Mean density $\bar{\rho}$ at $x/D=70$ (symbols as in Fig. 23).

Turbulent reacting flows can be described on the single-point level in terms of the velocity-scalar pdf.[77,78] Since the pdf contains considerably more statistical information than a finite set of statistical moments, the corresponding closure problem is quite different from the moment approach just described. The main advantage of the pdf approach in this form is the fact that turbulent diffusion and chemical reaction can be treated rigorously, because they appear in closed form. However, closure approximations are required for molecular transport (diffusion) and nonlocal pressure interactions. Pope[77,79] has done pioneering work in the closure of the velocity-scalar pdf and its solution by Monte Carlo methods. The current discussion will be focused on the closure of the molecular diffusion terms and an appropriate representation of the pdf for free shear flows undergoing chemical reaction. This can be done for the single-scalar pdf that is accessible to finite difference solution methods.

#### *PDF Equation*

The pdf of a scalar $\phi$ (varying in the unit interval) which is conserved and satisfies

$$\rho\partial_t\phi+\rho v_\alpha\partial_\alpha\phi=\partial_\alpha(\rho\Gamma\partial_\alpha\phi) \tag{17}$$

can be split into both singular and continuous parts

$$P(\psi)=P_1\delta(\psi)+P_2\delta(1-\psi)+(1-P_1-P_2)P_c(\psi) \tag{18}$$

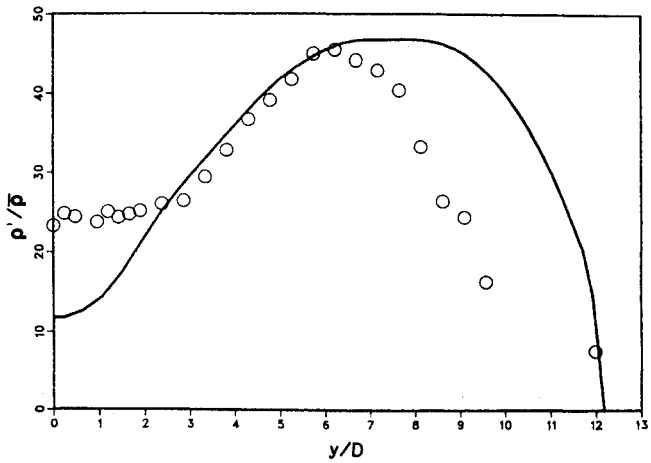


**Fig. 30 Normalized radial variation of the density fluctuations $(\overline{\rho'^2})^{1/2}/(\bar{\rho}_0 - \rho_e) \times 100$ (symbols as in Fig. 23).**

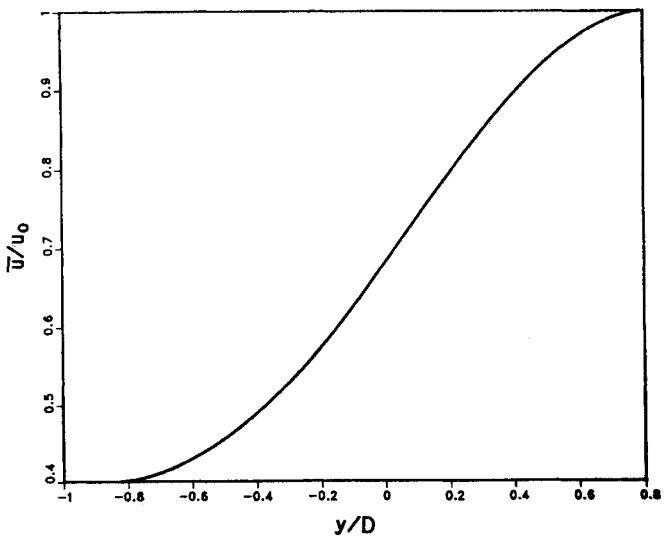


**Fig. 31 Normalized mean velocity $\bar{u}/u_0$ in plane reacting mixing layer at $x = 45$ cm downstream of splitter plate: $u_0 = 8.8$ m/s, $u_1 = 22$ m/s, equivalence ratio $\phi = 1$.**

The transport equations for the continuous part $P_c(\psi)$ and the coefficients of the singular parts $P_1$ and $P_2$ can be closed.[78] The critical assumptions are the gradient-flux model for the turbulent fluxes and a consistent scalar dissipation model[3,78] that includes explicit expressions for the interactions of the singular parts with themselves and the continuous part. Coupled with an appropriate turbulence closure, a prediction model for reacting flows (where the thermochemistry can be described by a single scalar) is obtained.

*PDF Model Prediction: Chemically Reacting Shear Layer*

The reacting plane mixing layer experiment of Mungal et al.[80,81] offers an excellent opportunity to apply the pdf model to a reacting flow because the heat release is significant, but not so strong that the density variations have a dominant influence. Furthermore, since large coherent structures appear in this reacting flow, further critical assessment of the ideas incorporated in the model is afforded. In the discussion that follows, the chemically reacting shear layer has been modeled by one of the present authors (Kollmann). His calculations are compared with the experimental temperature results obtained by Mungal.[80,81]

The chemical reaction in the layer is

$$H_2 + F_2 \rightarrow 2HF \tag{19}$$

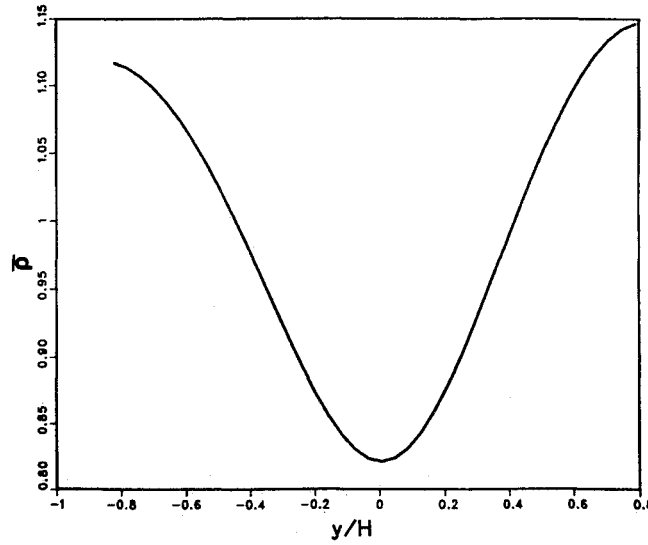


**Fig. 32 Mean density $\bar{\rho}$ in reacting mixing layer (same conditions as in Fig. 31).**

where each freestream contains either $H_2$ (1 or 2%) or $F_2$ (1, 2, or 8%) plus $N_2$ as an inert component. The reaction is fast enough that a single scalar variable can be used to describe it. Such a scalar vairable is defined by

$$f \equiv \frac{C_H - C_H^0}{C_H^1 - C_H^0} \tag{20}$$

where $C_H$ is the atomic mass fraction of hydrogen. Superscripts refer to the low-speed (0) and high-speed (1) sides of the mixing layer, respectively. Density, temperature, and composition then become local functions of the scalar $f$. The turbulence model used here is described in Ref. 67, except for the dissipation rate equation, which was replaced by the definition of the length scale

$$l \equiv K\,|y_{0.1} - y_{0.9}|$$

where $K = 0.93$ and $y_{0.1}$ and $y_{0.9}$ are the locations of

$$0.1\left|\frac{\tilde{u} - u_0}{u_1 - u_0}\right| \quad \text{and} \quad 0.9\left|\frac{\tilde{u} - u_0}{u_1 - u_0}\right|$$

It then follows that

$$\epsilon = k^{3/2}/l \tag{21}$$

All results reported were made for 2% $H_2$ in $N_2$ and 2% $F_2$ in $N_2$ (both by volume) and were obtained at $x = 45.72$ cm downstream from the splitter plate (same as in Ref. 80). The cross-flow coordinate is normalized by

$$\eta = (y - y_{0.5})/H \tag{22}$$

where $y_{0.5}$ is the halfwidth of the $\tilde{f}$ profile and $H$ is the thickness of the temperature profiles as defined in Ref. 80. Calculations were started assuming thin (laminar) boundary layers on both sides of the plate. The equivalence ratio $\phi$ is the ratio of reactant mole fractions in the freestreams.

Case $\phi = 1$. Figures 31-35 give an overview of the flow by representing normalized mean velocity $\tilde{u}/u_0$ (Fig. 31), mean density $\bar{\rho}$ (Fig. 32), and mean temperature $\tilde{T}$ (Fig. 33) plotted in normalized form as

$$(\tilde{T} - T_{min})/(T_{ad} - T_{min}) \tag{23}$$

where $T_{ad}$ is the adiabatic flame temperature and $T_{min}$ the ambient (minimum) temperature. In Fig. 33, model predictions for 1% $H_2$ of normalized mean temperature are compared

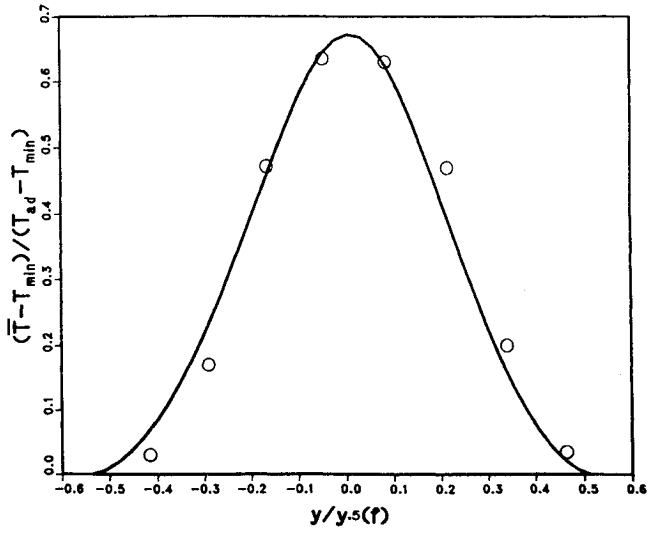


Fig. 33 Normalized mean temperature in reacting mixing layer (same conditions as Fig. 31). Symbols: experiments of Mungal[80] for 1% vol. $H_2$.

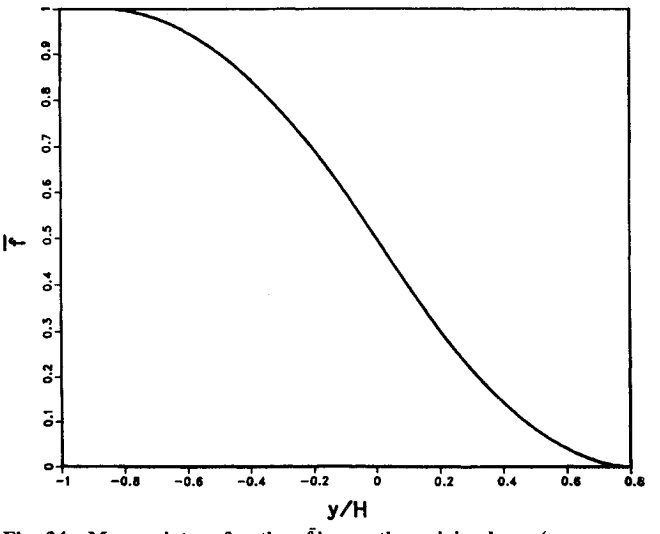


Fig. 34 Mean mixture fraction $\bar{f}$ in reacting mixing layer (same conditions as Fig. 31).

with the experimental results of Mungal. Mean and variance of the scalar $f$ are shown in Figs. 34 and 35. The continuous part of the pdf $P(f)$ is shown in Fig. 36 for several radial stations.

Case $\phi = 1/8$. The mean temperature profile and the pdf at several stations are presented in Figs. 37 and 38. Of most interest is the comparison with Mungal's experiments in Fig. 37. Skewness of the profile is due to the functional form of $T(f)$ and is not due to a closure assumption.

Case $\phi = 8$. Model predictions are presented as before in Figs. 39 and 40. For this case, the mean temperature appears to be in good agreement with the experimental (for 1% $H_2$). Skewness in the profile is again a consequence of $T(f)$. The form of the pdf in all three cases shows the typical relative maximum, which cannot be represented by the beta function. This is not due to chemical reaction, but to the different phases of mixing: entrainment and progress of molecular diffusion.[82] Calculations for passive scalars confirmed the ability of the model to reproduce bi- and tri-modal pdf's[78] resulting from these processes.

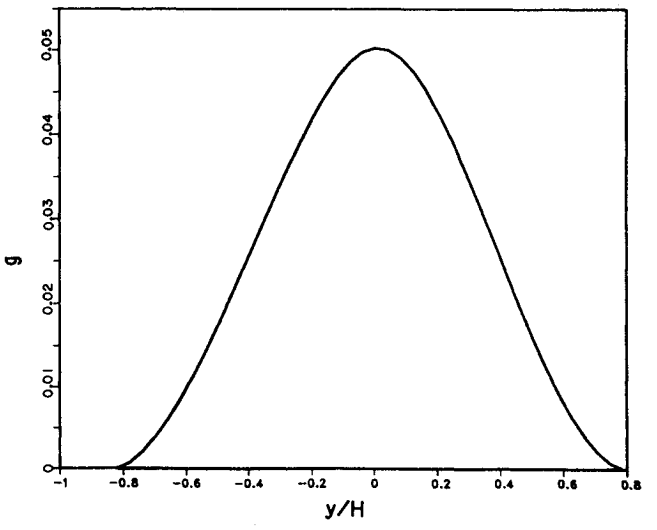


Fig. 35 Variance of mixture fraction $g \equiv \overline{f'^2}$ in reacting mixing layer (same conditions as Fig. 31).

### Vortex Dynamics Approach

Time-dependent turbulent flow simulation has become possible with the arrival of supercomputers, but only at modest levels. The time-dependent turbulence simulation approaches can be divided into three categories: 1) direct numerical simulation of the Navier-Stokes equations; 2) large eddy simulation, where the larger length scales are captured and the effects of the smaller length scales on the large length scales are modeled; and 3) numerical simulation of discrete vortex dynamics.

Direct numerical simulation of turbulent, nonreacting flow has been extended to include $128^3$ points[83] and shows promise of revealing time-dependent flow structure. Grötzbach[84] has studied unsteady heat transfer at large Rayleigh numbers and has developed three criteria for the grid selection.

Large eddy simulation of turbulent channel flow with a similar number of grid points has reproduced the observed wall flow structure.[85] With some confidence, certain details of these computed structures can be examined beyond what is experimentally possible. Kim[86] has studied the effect of global rotation on channel flow and found, in agreement with experiment, that rotation stabilizes one wall flow and destabilizes the other. On the unstable wall, the shear stress increase was produced by an increase in the numer of streak flow structures per unit area.

The early vortex dynamics work included the simulation of two-dimensional mixing layers and showed that the deter-

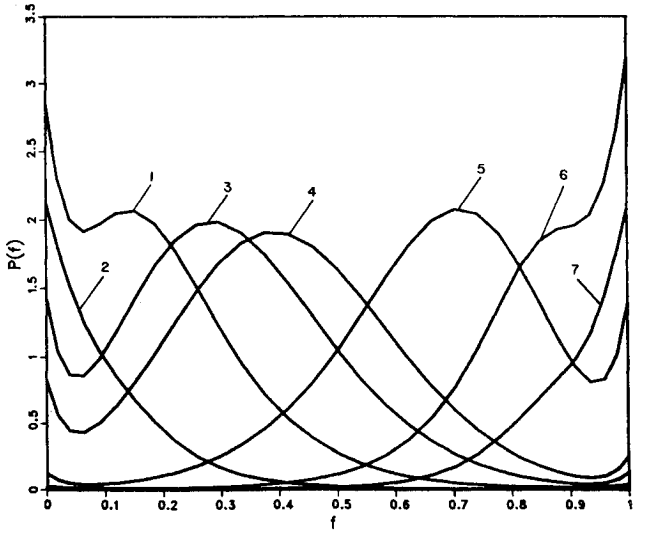


Fig. 36 Pdf of mixture fraction at $x = 45$ cm and at locations $y$ for $\bar{f} = 0.97(1)$, $0.9(2)$, $0.7(3)$, $0.4(4)$, $0.3(5)$, $0.15(6)$, and $0.03(7)$.

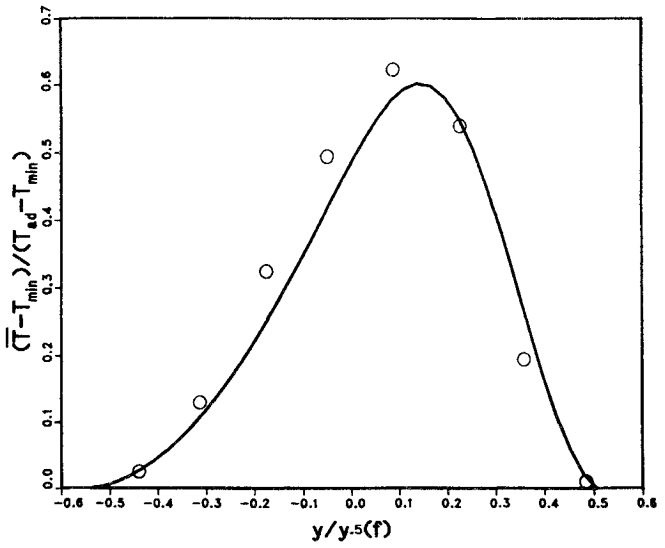


Fig. 37 Normalized mean temperature in reacting shear layer (same conditions as Fig. 31 except $\phi = 1/8$). Symbols: experiments of Mungal.[80]

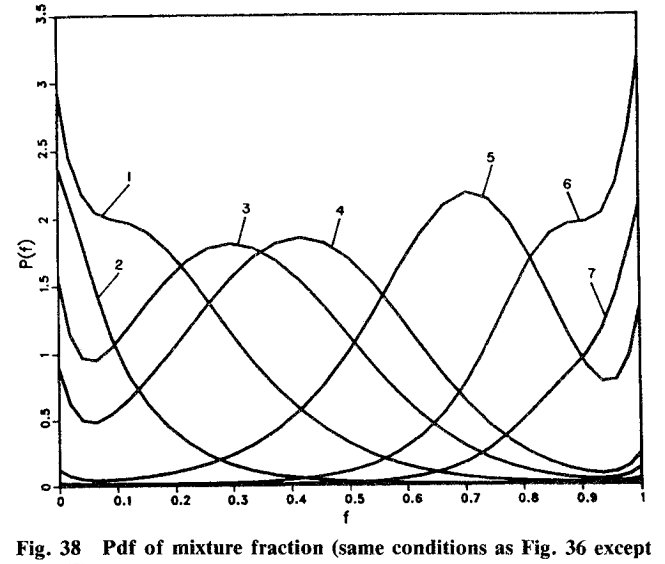


Fig. 38 Pdf of mixture fraction (same conditions as Fig. 36 except $\phi = 1/8$).

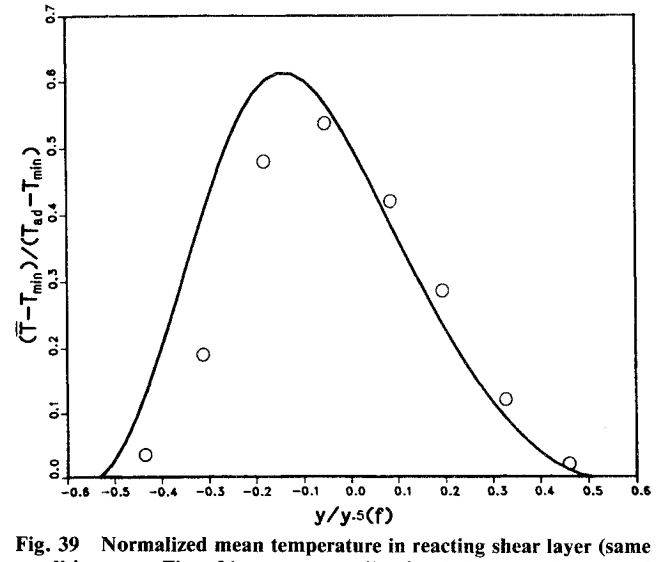


Fig. 39 Normalized mean temperature in reacting shear layer (same conditions as Fig. 31 except $\phi = 8$). Symbols: experiments of Mungal.[80]

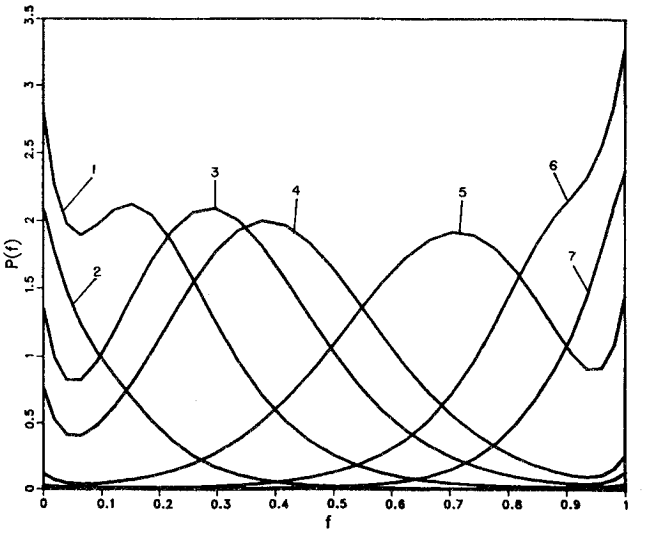


Fig. 40 Pdf of mixture fraction (same conditions as Fig. 36 except $\phi = 8$).

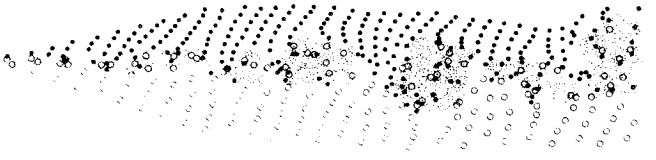

Fig. 41 Entrainment in a planar mixing layer depends upon the vorticity structure.

ministic entrainment structure is of vital importance in explaining phenomena such as flame liftoff in a turbulent diffusion flame. In Fig. 41, the calculated marking particle motion reveals the entrainment pattern. The instantaneous plot in Fig. 41 shows the discrete vorticity regions (shaded areas) and Lagrangian marker particles that start in the top fluid (solid circles) and in the bottom (open circles). The faster flow is on the bottom and is carried across the layer on the downstream side of the vorticity regions, which rotate counterclockwise, while the slow flow from the top enters the layer on the upstream side. The majority of the fluid mixing occurs in the spirals of the vortex cores, which exhibit three-dimensional motion in experiments.

In the vortex dynamics method, vorticity is used to describe the velocity field at any desired location. This vorticity is discretized and is advanced in time in a Lagrangian coordinate system and thus represents a self-adapting grid for the velocity field. Because fluids have finite viscosity, vorticity is created whenever there is relative motion past obstacles. In the computer work described here, vorticity is either created continuously at the wall boundaries or created initially. The final choice depends on the problem of interest. For reacting flow studies, wall-bounded flows are not used. Thus, the focus is on systems having initial vorticity and the effect of this vorticity on convecting a scalar (which also diffuses and possibly reacts). The effect of vortex stretching is not included since the flows are two-dimensional. Thus, the turbulence cascade is not properly simulated. However, by varying the vortex parameters, mixing flows can be constructed with length and velocity scales of interest to reacting flows, e.g., a flow length scale much greater than or comparable to the reaction zone thickness. Discrete vortices will thus provide turbulent convection velocities, while a reacting, diffusing scalar will be calculated on a fixed Eulerian mesh.

*Conserved-Scalar Diffusion*

In this work, there is no explicit chemical reaction; instead, a conserved scalar is convected and diffused. For a diffusion

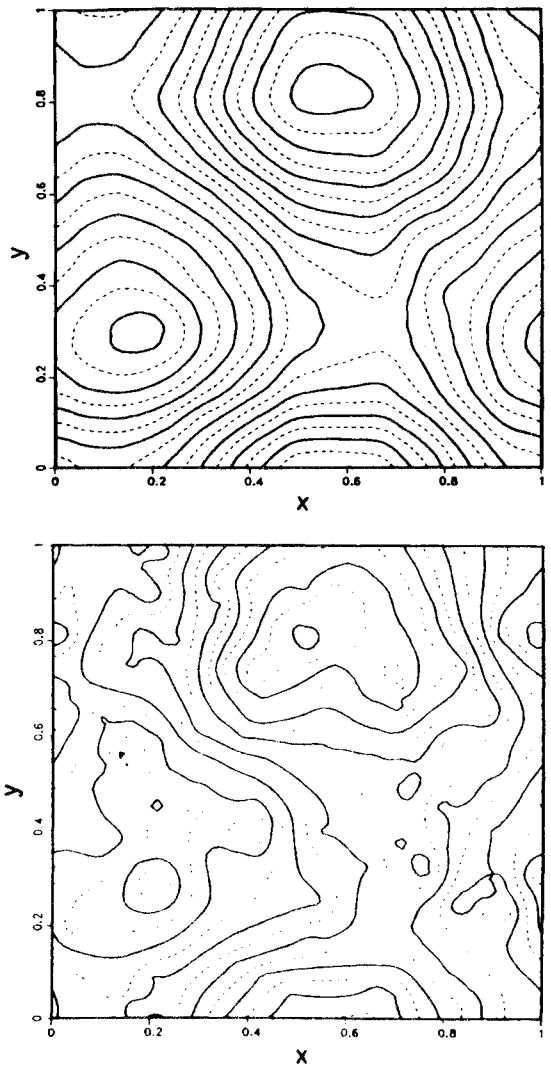


**Fig. 42 Stream function contours in a periodic two-dimensional flow show the flow length scale dependence upon discrete vortex core parameter. The smooth flow (top) is achieved with large-core vortices and the more chaotic flow with small cores; largest core value is ⅓ and 1/100 of the square edge, respectively.**

**Fig. 43 Representative scalar contours and vorticity locations at dimensionless time 1.3. The rotation is counterclockwise, so flow is down on the left side of the layer and up on the right side with a velocity difference of unity across the layer. The 200 discrete vortices are shown by their velocity vectors. From left to right the scalar contour values are 0.99, 0.5, 0.2, 0.15, 0.10, 0.05, and 0.01.**

flame, in the limit of fast chemistry, the time-averaged chemical reaction rate will be dependent on the time average of the scalar dissipation, which is the square of the scalar gradient times the molecular diffusion coefficient. The physical reason for this dependence is that in a flame reaction zone there is a balance between the loss of heat and mass by conduction and the creation of heat from chemical reaction. The flame will be located near the stoichiometric isopleth unless the thermal gradient is too large. With a large gradient, sufficient heat is transported away from the reaction zone that the temperature drops and the (exponentially sensitive) reaction rate decreases to zero. This process can result in local extinction of the flame. The purpose of the work described here is to obtain statistical information on the scalar gradient and compare it with the assumptions that have been used in past conserved-scalar analysis of turbulent diffusion flames (for a review, see the chapter by Bilger in Ref. 49). One of these assumptions is that the dissipation is independent of the scalar value. If it is not independent, then what is the distribution of dissipation?

These calculations use 200 discrete vortices interacting in a square of side length $L$. Each vortex has a circulation strength $\Gamma$ and a nonzero core size $r_{core}$ that produces a rigid-body rotation at the vortex location, but changes to the potential point vortex field at large distance from the vortex. With one exception, the velocity field is periodic in both directions, with only the nearest vortex image used to calculate the vortex velocity. The dynamics of the vortices, calculated in a Lagrangian frame, evolves completely independent of the scalar dynamics, which is calculated on a fixed Eulerian mesh. From the known vortex positions, the vortex-induced stream function is calculated at the grid cell corners of an $80 \times 80$ mesh. Subtraction of two adjacent stream function values yields the average cell-face velocity to be used in fluxing the scalar through that cell face. Examples of such grid-calculated stream functions are shown in Fig. 42, where the effect of the core parameter can be seen to change the flow length scales. Smaller core sizes yield a higher Reynolds number flow pattern.

Zalesak's[87] flux-corrected transport is used to convect and diffuse the scalar. This technique uses two convection schemes: one low order and diffusive and the other high order to obtain convection with steep gradients without exceeding local maximum and minimum values of the scalar.

*Homogeneous Flow*

A homogeneous flow is created by picking a random number seed and randomly distributing the 200 vortices in the square. Vortex circulation and core size are also randomly selected with prescribed bounds. The stream function pattern changes in time, but not in any statistically significant way; i.e., the beginning and ending patterns look alike. Ensemble averages are achieved by changing the random number seed and rerunning the problem.

1) *Scalar Spot.* In these calculations, a spot of scalar is created at time zero and the maximum scalar value is monitored as a function of time. Comparison is made with the time rate of change that laminar diffusion only would accomplish. In this manner, an apparent turbulent diffusion coefficient can be defined. For the conditions examined, a diffusion enhancement of up to five times laminar occurs with a linear dependence on the flow field root mean square (rms) velocity and a linear slope dependent on the flowfield length

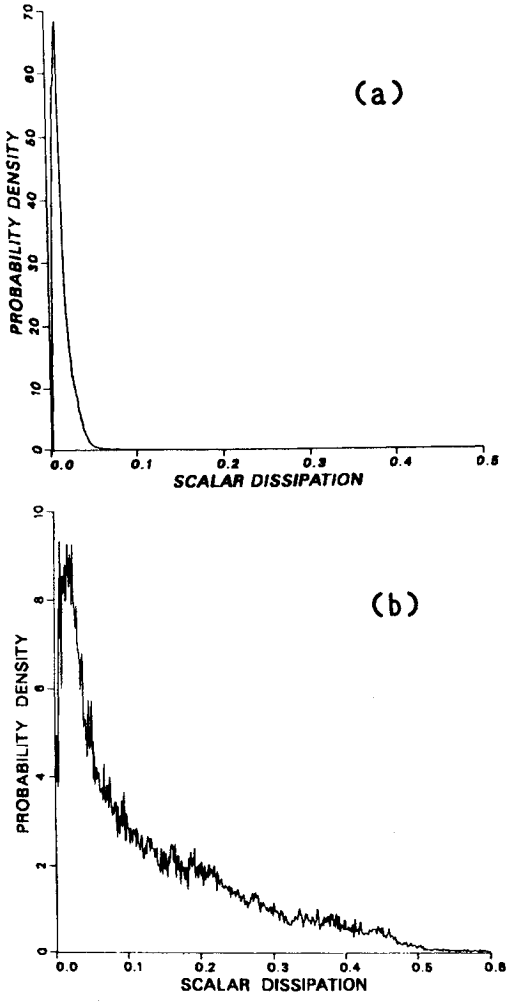


**Fig. 44 Probability distribution function of the dimensionless scalar dissipation as a function of scalar value in the mixing layer. The scalar values are 0.05 and 0.50 for a) and b), respectively. Note the larger spreading associated with the larger scalar value.**

scales. Smaller length scales and larger rms yield faster dissipation of the original scalar spot.[88] (This is the same functional form that is found in the premixed flame work described later.)

2) *Constant Scalar Gradient.* In the spot problem, the periodic boundaries and the initial spot amplitude limit the observation time. Thus, a nonequilibrium periodic boundary system was developed. At time zero, the scalar is distributed such that the scalar value changes from unity to zero in the $x$ direction. Scalar boundary conditions are periodic in the $y$ direction, but a jump by $\pm 1$ occurs in the $x$ direction. In this system, neither diffusion nor convection can bring the scalar to a spatially uniform value. At a time after zero, when the scalar has lost the features of the initial conditions, the scalar gradient is calculated in the center of each grid cell using a bilinear fit of scalar values. The correlation of the dissipation with the scalar value is found to be negative and small, but not zero. Thus, dissipation is not quite independent of the scalar value. The distribution of scalar dissipation is found to be log normal (i.e., the logarithm of the variable is Gaussian). Futhermore, the log normal parameters, mean and variance, depend on the sample size in the manner predicted by Gurvich and Yaglom.[89] Different sample sizes are achieved by averaging together the calculated dissipation in $n \times n$ cells before creating the distribution. Details of this work are given in Ref. 89.

*Inhomogeneous Flow*

An inhomogeneous flow was created to resemble a mixing layer: all the vorticity has the same circulation strength and

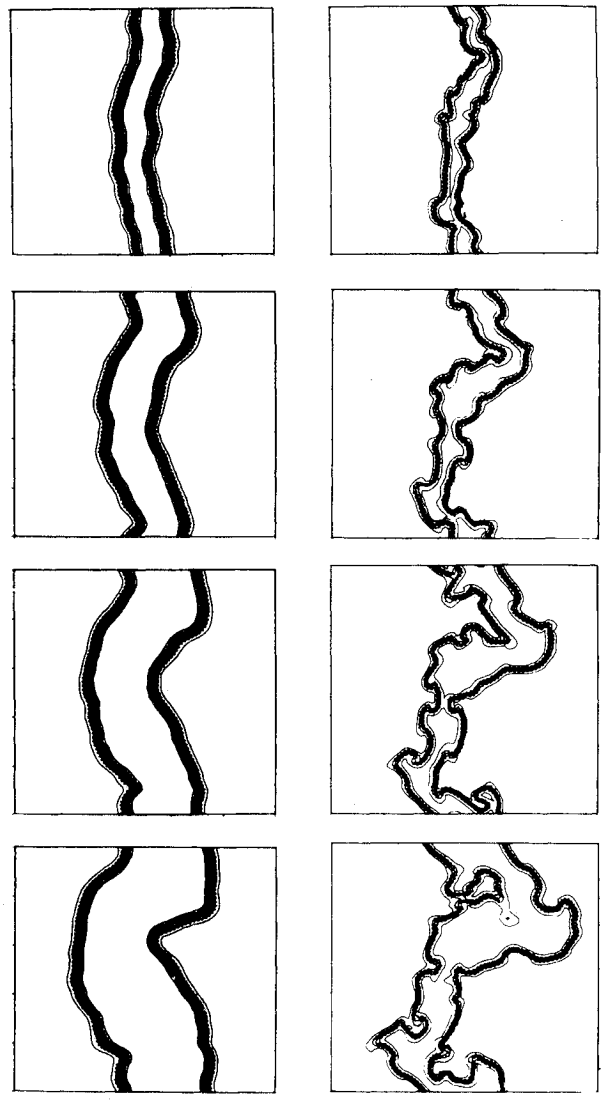

**Fig. 45 Development of flame surface in the flowfield shown in Fig. 43. Temperature contours are shown at four times after ignition. The center is hot and flames propagate to the right and left and are connected at the top and bottom by a periodic boundary condition. In the smaller length scale flow (right column), the consumption rate is almost twice that of the smoother flame (left column).**

sign and is initially randomly distributed along the $y$ axis. The total circulation is unity, so that there is a unit change in the $y$ velocity from one side of the system to the other in the $x$ direction. The velocity and stream function are no longer periodic in the $x$ direction. Thus, the large-scale structure associated with the two-dimensional mixing layer develops in this system, but only up to length scales of order $L$, where the periodic $y$ direction limits the growth. A typical pattern is shown in Fig. 43. Statistics are gathered during a time period before the periodic length affects the vortex motion and after the initial conditions have vanished.

At time zero, the scalar is set to unity for negative $x$ and to zero for positive $x$. The line of discrete vorticity is thus the scalar boundary and has a scalar value of one-half. In this inhomogeneous system, it is not possible to average in the $x$ direction in a statistically correct manner because there is no unique distance from the layer in this "free" boundary direction. Of course, statistics can still be obtained from averages in the periodic $y$ direction. Therefore, statistics of scalar dissipation are obtained by marching along scalar isolines and for a given gradient range, i.e., a particular bin size of the discrete pdf, the quantity of the isoline length in that particular grid cell times the inverse of the gradient is accumulated, which yields the proper volumetric averaging.

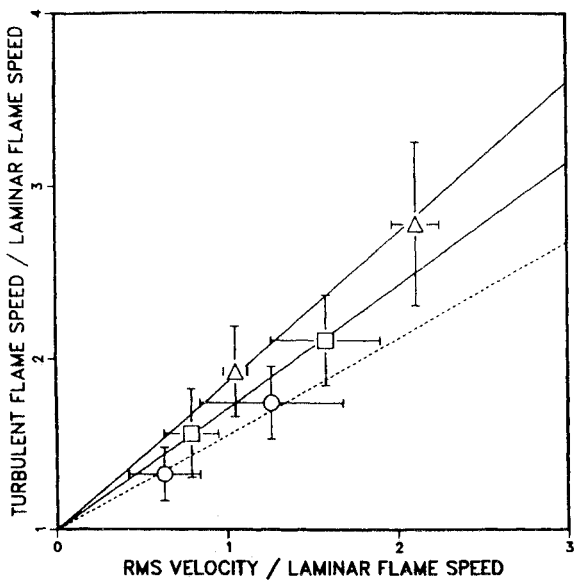


**Fig. 46 Calculated turbulent flame speeds using the finite-thickness model follow the linear relation suggested by the wrinkled laminar flame model (one standard deviation of the calculated values are indicated by the error bars). Lines are drawn through the origin with a slope corresponding to the average slope of the results at fixed length scale. The dashed line represents the case of all vortices with the same core size: 0.32 $L$, where $L$ is the edge length of the squares shown in Fig. 45. The middle line results have a large vortex core range (uniform distribution between 0 and 0.32 $L$), whereas the upper line connects results calculated with a maximum core size of 0.01 $L$. Thus, decreasing the core size, which corresponds to increasing the Reynolds number, increases the flame speed.**

The scalar dissipation distribution depends on the scalar value: for small scalar values (i.e., by diffusion these isolines are removed from the middle of the mixing layer), the pdf is log normal with mostly small values of dissipation, while near the interior of the layer the dissipation is only approximately log normal and has values spread over a much wider range (Fig. 44).

A very simple model explains much of the observed dissipation dependence on the scalar value. Given the step initial conditions, then if there were no two-dimensional convection, the exact solution would be the error function solution of the unsteady one-dimensional diffusion equation. It is assumed that two-dimensional effects can be approximated with a log normal variable and further that this new stretching variable multiplies the one-dimensional solution. With these assumptions, it is possible to arrive at the log normal parameters for the dissipation with an explicit scalar dependence. Comparison with the calculated results indicate that this stretching model is useful for scalar values less than 0.3. Larger scalar values occupy the region of the mixing layer where flow structure dominates in twisting the scalar isolines (contour islands appear due to convection and disappear due to diffusion). Thus, failure of a modified one-dimensional solution at large scalar value is reasonable when the two-dimensional effects are so large. However, for combustion applications, it is the low scalar values that are of interest, since the flame zone would be in the neighborhood of the 0.05 isoline. More details are given in Ref. 90. Experiments are in progress to measure the scalar dissipation using Rayleigh scattering and a one-dimensional reticon-array detector.[25]

*Premixed Flames*

When the fuel and oxidizer are premixed, then finite-rate chemistry must be calculated and the conserved scalar approach no longer applies. Two different approaches have been followed in this work: 1) calculate flame structure for specified chemical kinetics; and 2) replace the thin flame with an interface that moves into the unburned fluid with a specified velocity, which may depend on the flame curvature. In the limit of wrinkled laminar flames, these two methods give the same functional results for premixed flame speed dependence on turbulent flow parameters. First, the flame structure work will be described.

Reacting scalar work has so far been restricted to the simplest possible kinetic scheme: a single species reacts to products depending only on the amount of the species and the temperature. The kinetic parameters (collison rate and activation energy) have been selected so that the flame zone can be resolved on an $80 \times 80$ mesh. The flame is about five mesh cells thick.

The initial work ignored the effect of heat release on the flow. Therefore, the vortex dynamics is independent of chemistry. The justification of such a calculation lies in its simplicity and the possibility of comparing it to theoretical work with the same assumptions. Later work included the volume expansion effect on the vortex motion, but not the vorticity source caused by density gradients combined with fluctuating pressure gradients. These calculations are restricted to two dimensions and, therefore, the vortex stretching effects are not included. To approximate a two-dimensional slice from a three-dimensional fluid volume, a range of vortex core sizes are used to allow a range of flow length scales.

In these two-dimensional, periodic systems the turbulent flame speed is defined by the disappearance rate of fuel, averaged over the system. A strip ignition creates two flame fronts that are connected by the periodic $y$ direction boundary. At some later time, the two fronts will also interact in the $x$ direction because of the other periodic boundary. It is before this latter time that the fuel consumption rate is determined and the apparent flame speed is defined. A typical time development is shown in Fig. 45. The flowfield on the left has only large-core vortices and would correspond to a low Reynolds number flow, in comparison to the flow on the right that has a core range 30 times smaller. The effect on the flame surface is evidenced by the more intense wrinkles that develop. Ensemble averages in such systems yield the flame speed results shown in Fig. 46. The lines connect results that have the same flow length scales, but differ in the rms velocity. It is concluded that turbulent flame speed is linear in the rms velocity with the coefficient depending on the turbulent length scales. This is in agreement with the experimental correlation published by Bradley.[91]

For inclusion of the density expansion, the system boundaries are changed to inflow/outflow in the $x$ direction. The apparent flame speed did not change in the range of rms velocities examined in the periodic system work.

To investigate the question of flame structure and its possible change in a turbulent flow, a series of calculations were done with flame structure replaced by a thin interface that propagates into the unburned fluid with constant velocity. Flame speed results with this model were in agreement with Fig. 46, within the rather large error bars. Thus, it is concluded that the enhanced turbulent flame speed is due to the turbulent flow creating more flame surface rather than increasing transport within the flame structure (see Ref. 92).

Further work will continue in two dimensions, but will include the density gradient effects on the vorticity field and determine statistics of the velocity field that enter the time-averaged turbulence models of premixed flames.

## Conclusions

Much of our current knowledge of turbulence is based on observations made in constant-density flows. Although the present predictive capabilities in nonreacting, constant-density flows are impressive, some outstanding problems still remain. These problems are exacerbated when the complexities of combustion are combined with fluid-dynamical turbulence.

For example, how does turbulence change when there are large variations in gas density as are created by a flame? Or, how does one accommodate the exponential variation of chemical reaction rate in circumstances where there are large spatial and temporal variations in gas temperature? As with constant-density turbulence, it is anticipated that progress will continue as a result of observations, both qualitative and quantitative, made on turbulent combustion experiments. Fortunately, the increased complexity of the problem is ameliorated somewhat by recent advances in combustion diagnostics and computational capabilities. The purpose of this paper has been to present several examples of these improved capabilities, which remain in various stages of development.

From an experimental viewpoint, Rayleigh and Raman scattering are well understood relative to more advanced techniques such as coherent anti-Stokes Raman spectroscopy and inverse Raman scattering. Simultaneous measurement of velocity, along with major species, temperature, and density using laser velocimetry combined with Rayleigh or Raman scattering, is in an intermediate stage of development. For example, LV-Rayleigh and Raman have been used extensively in nonhydrocarbon flames and are currently being extended to hydrocarbon-fueled flames.[93,94] Although not specifically discussed in the paper, similar simultaneous measurement of minor and radical species along with major species and velocity is possible; techniques to make these measurements are currently under development at several laboratories. Since the original draft of this paper was written, there has been significant progress in this area. For example, simultaneous planar Rayleigh and $C_2$ fluorescence measurements have been obtained in a turbulent methane-air flame to record the spatial and temporal distribution of temperature and flame location, respectively.[94] Also, simultaneous imaging of methane and oxygen concentrations in a bluff-body stabilized turbulent flame have been obtained recently.[95] When these simultaneous point-measurement techniques are combined with the emerging planar-imaging techniques, experimentalists will have an impressive inventory of tools to bring to bear on the problem of turbulent combustion.

From a modeling viewpoint, the last five years have seen a steady improvement in moment and pdf models, as exemplified by the emergence of predictions of differential diffusion, departures of radical species from chemical equilibrium, and, more recently, departures of major species as from chemical equilibrium as well. The ability of the moment approach to calculate the properties of a turbulent jet flame and the ability of the pdf approach to reasonably calculate temperature distributions in a chemically reacting shear layer have been demonstrated in this paper. Comparable predictions using vortex dynamics await further development. Nevertheless, interest in the vortex approach is strong and growing because important fundamental features of fluid turbulence (as opposed to the overlying chemistry) are explicitly represented by vortex dynamics; these features are, at best, implicitly represented by moment models.

## Acknowledgment

This work was supported by the U.S. Department of Energy, Office of Basic Energy Sciences.

## References

[1]Bray, K. N. C., *Seventeenth Symposium (International) on Combustion*, The Combustion Institute, Pittsburgh, PA, 1979, p. 223.

[2]Gosman, A. D., Lockwood, F. C., and Salooga, A. P., *Seventeenth Symposium (International) on Combustion*, The Combustion Institute, Pittsburgh, PA, 1979, p. 747.

[3]Janicka, J., Kolbe, W., and Kollmann, W., *Journal of Non-Equilibrium Thermodynamics*, Vol. 4, 1979, p. 47.

[4]Libby, P. A. and Williams, F. A., *AIAA Journal*, Vol. 19, March 1981.

[5]Yanagi, T. and Mimura, Y., *Eighteenth Symposium (International) on Combustion*, The Combustion Institute, Pittsburgh, PA, 1981, p. 1031.

[6]Moss, J. B., *Combustion Science and Technology*, Vol. 22, 1980, p. 119.

[7]Driscoll, J. F., Schefer, R. W., and Dibble R. W., *Nineteenth Symposium (International) on Combustion*, The Combustion Institute, Pittsburgh, PA, 1983, pp. 477-487.

[8]Namazian, M., Talbot, L., and Robben, F., *Nineteenth Symposium (International) on Combustion*, The Combustion Institute, Pittsburgh, PA, 1983, pp. 487-495.

[9]Dibble, R. W. and Hollenbach, R. E., *Eighteenth Symposium (International) on Combustion*, The Combustion Institute, Pittsburgh, PA, 1981, p. 1489.

[10]Warshaw, S., Lapp, M., Penney, C. M., and Drake, M. C., *Laser Probes for Combustion Chemistry*, edited by D. R. Crosley, Symposium Series, No. 134, American Chemical Society, Washington, DC, 1980, p. 207.

[11]Drake, M. C., Lapp, M., Penney, C. M., Warshaw, S., and Gerhold, B. W., *Eighteenth Symposium (International) on Combustion*, The Combustion Institute, Pittsburgh, PA, 1981, p. 1521.

[12]Dibble, R. W., Kollmann, W., and Schefer, R. W., *Combustion and Flame*, Vol. 55, 1984, p. 307.

[13]Drain, L. E., *The Laser Doppler Technique*, John Wiley & Sons, New York, 1980.

[14]Durst, F., Melling, A., and Whitelaw, J. H., *Principles and Practice of Laser Doppler Anemometry*, Academic Press, New York, 1976.

[15]Self, S. A. and Whitelaw, J. H., *Combustion Science and Technology*, Vol. 13, 1976, p. 171.

[16]Graham, S. C., Grant, A. J., and Jones, J. M., *AIAA Journal*, Vol. 12, 1974, p. 1140-1142.

[17]Hartley, D. L., *AIAA Journal*, Vol. 10, May 1972, p. 687-689.

[18]Smith, J. R., and Geidt, W. H., *International Journal of Heat and Mass Transfer*, Vol. 20, 1977, pp. 899-910.

[19]Lapp, M. and Penney, C. M. (eds.) *Laser Raman Gas Diagnostics*, Plenum Press, New York, 1974.

[20]Goulard, R. (ed.), *Combustion Measurements*, Academic Press, New York, 1976.

[21]Crosley, D. R. (ed.), *Laser Probes for Combustion Chemistry*, Symposium Series, No. 134, American Chemical Society, Washington, DC, 1980.

[22]Smith, J. R., "Instantaneous Temperature and Density by Spontaneous Raman Scattering in a Piston Engine," AIAA Paper 80-1359, 1980.

[23]Drake, M. C., Bilger, R. W., and Starner, S. H., *Nineteenth Symposium (International) on Combustion*, The Combustion Institute, Pittsburgh, PA, 1983, p. 459.

[24]Gouldin, F. C. and Dandekar, K. V., AIAA Paper 82-0036, 1982.

[25]Dibble, R. W., Kollmann, W., Schefer, R. W., and Hartmann, V., "Scalar Dissipation in Turbulent Reacting Flows: Modeling and Measurement," *Twentieth Symposium (International) on Combustion*, 1984, p. 345.

[26]Smith, J. R., *SAE Transactions*, Vol. 91, 1982, p. 150.

[27]Koochesfahani, M. M., Ph.D. Dissertation, California Institute of Technology, Pasadena, 1983.

[28]Kychakoff, G., Howe, R. D., Hanson, R. K., and McDaniel, J. C., *Applied Optics*, Vol. 21, 1982, pp. 3225-3227.

[29]Long, M. B., Fourguette, D. C., and Escoda, M. C., *Optics Letters*, Vol. 8, No. 5, 1983.

[30]Rahn, L. A., Mattern, P. L., and Farrow, R. L., *Eighteenth Symposium (International) on Combustion*, The Combustion Institute, Pittsburgh, PA, 1981, pp. 1533-1542.

[31]Namer, I. et al., "Interaction of a Plane Flame Front with the Wake of a Cylinder," Paper presented at Fall Meeting, Western States Section, The Combustion Institute, Oct. 1977.

[32]Schefer, R. W., Robben, F., and Cheng, R. K., *Combustion and Flame*, Vol. 38, No. 1, 1980, p. 51.

[33]Muller-Dethlefs, K. and Weinberg, F. J., *Seventeenth Symposium (International) on Combustion*, The Combustion Institute, Pittsburgh, PA, 1979, p. 985.

[34]Dyer, T. M., *AIAA Journal*, Vol. 17, 1979, pp. 912-914.

[35]Dyer, T. M., *SAE Transactions*, Vol. 88, 1979, p. 1196.

[36]Smith, J. R., "Rayleigh Temperature Profiles in a Hydrogen Diffusion Flame," *Proceedings of the Society of Photo-Optical Instrumentation Engineers*, Vol. 158, 1978, p. 85.

[37]Lederman, S., *Progress in Energy and Combustion Sciences*, Vol. 3, No. 1, 1977.

[38]Eckbreth, A. C., *Eighteenth Symposium (International) on Combustion*, The Combustion Institute, Pittsburgh, PA, 1981, p. 1471.

[39]Yaney, P. P., Gallis, M., Danset, P., and Perez, J., "Dynamic Measurements in Gas Flowfields Using Rotational Raman Spectroscopy," Paper presented at 9th International Colloquium of Dynamics of Explosions and Reactive Systems, Poitiers, France, 1983.

[40]Aeschliman, D. P., Cummings, J. C., and Hill, R. A., *Journal of Quantitative Spectroscopy & Radiative Transfer*, Vol. 21, 1978, pp. 293-307.

[41]Smith, J. R., *SAE Transactions*, Vol. 89, 1980, p. 808.

[42]Eckbreth, A. C., Bonczyk, P. A., and Verdieck, J. F., *Progress in Energy and Combustion Sciences*, 1979, p. 253.

[43]Bilger, R. W., *AIAA Journal*, Vol. 20, 1982, p. 962-970.

[44]Mitchell, R. E., "Chemical Element Diffusion Factors for Use in the Conserved Scalar Approach to Diffusion Flame Modeling," Paper presented at Fall Meeting, Western States Section, The Combustion Institute, 1980.

[45]Reynolds, W. C., "STANJAN: Interactive Computer Programs for Chemical Equilibrium Analysis," Thermosciences Div., Dept. of Mechanical Engineering, Stanford University, Stanford, CA, 1981.

[46]Kollmann, W., "Mass Transport in Turbulent Flames," Paper presented at the AIChE Meeting, Los Angeles, Nov. 1982.

[47]Jones, W. P., *Prediction Methods for Turbulent Flows*, edited by W. Kollmann, Hemisphere, Publishing Corp., New York, 1980, p. 380.

[48]Pope, S., *Proceedings of the Royal Society of London,* Ser. A, Vol. 291, No. 9, 1979, p. 52.

[49]Libby, P. A. and Williams, F. A., *Turbulent Reacting Flows*, Springer-Verlag, New York, 1980, p. 14.

[50]Bilger, R. W., *Turbulent Reacting Flows*, edited by P. A. Libby and F. A. Williams, Springer-Verlag, New York, 1980, p. 65.

[51]Bilger, R. W., Antonia, R. A., and Sreevivasan, K. R., *The Physics of Fluids*, Vol. 19, 1976, p. 19.

[52]Antonia, R. A., Prabhu, A., and Stephenson, S. E., *Journal of Fluid Mechanics*, Vol. 72, Pt. 3, 1975, p. 455.

[53]Antonia, R. A., *Annual Review of Fluid Mechanics,* Vol. 13, 1981, p. 131.

[54]Libby, P. A., Chigier, N. A., and La Rue, J. C., *Progress in Energy and Combustion Sciences,* Vol. 8, 1982, pp. 203-231.

[55]Kennedy, I. M. and Kent, T. H., *Seventeenth Symposium (International) on Combustion*, The Combustion Institute, Pittsburgh, PA, 1979, p. 279.

[56]Bilger, R. W., *Progress in Energy and Combustion Sciences*, Vol. 1, 1976, p. 87.

[57]Goulard, R., Mellor, A. M., and Bilger, R. W., *Combustion Science and Technology,* Vol. 14, 1976, p. 195.

[58]Jones, W. P. and Whitelaw, J. H., *Combustion and Flame,* Vol. 48, 1982, p. 1.

[59]Bilger, R. W., *Combustion Science and Technology,* Vol. 13, 1976, p. 155.

[60]Bilger, R. W., *Progress in Energy and Combustion Sciences,* Vol. 1, 1976, p. 87.

[61]Bilger, R. W., *Combustion Science and Technology,* Vol. 22, 1980, p. 251.

[62]Janicka, J. and Kollmann, W., *Seventeenth Symposium (International) on Combustion*, The Combustion Institute, Pittsburgh, PA, 1979, p. 421.

[63]Bray, K. N. C., *Turbulent Reacting Flows,* Vol. 44, edited by P. A. Libby and F. A. Williams, Springer-Verlag, New York, 1980, p. 115.

[64]Bray, K. N. C., Libby, P. A., and Moss, J. B., "Unified Modeling Approach for Premixed Turbulent Combustion," *Combustion and Flame.*

[65]Jones, W. P. and Launder, B. E., *International Journal of Heat and Mass Transfer*, Vol. 15, 1972, p. 301.

[66]Jones, W. P., *Prediction Methods for Turbulent Flows,* edited by W. Kollmann, Hemisphere Publishing Corp., New York, 1980, p. 380.

[67]Janicka, J. and Kollmann, W., "A Prediction Method for Turbulent Diffusion Flames Including NO-Formation," AGARD Proc. 275, 1980.

[68]Janicka, J. and Lumley, J. L., "Second-Order Modeling in Non-Constant Density Flows," Cornell University, Ithaca, NY, Rept. FDA81-01, 1981.

[69]Farschi, M. and Kollmann, W., "Reynolds-Stress Closure for Turbulent Flames," Paper presented at ASME-AIChE Meeting, Seattle, 1983.

[70]Daly, B. J. and Harlow, F. H., *The Physics of Fluids,* Vol. 13, 1970, p. 2634.

[71]Launder, B. E. and Morse, A., "Numerical Prediction of Axisymmetive Free Shear Flows with a Second-Order Reynolds Stress Closure," *Turbulent Shear Flows I,* edited by F. Durst et al., Springer-Verlag, New York, 1979, p. 279.

[72]Kent, J. H. and Bilger, R. W., *Sixteenth Symposium (International) on Combustion,* The Combustion Institute, Pittsburgh, PA, 1977, p. 1643.

[73]Hanjalic, K. and Launder, B. E., *Journal of Fluid Mechanics*, Vol. 52, 1972, p. 609.

[74]Kennedy, I. M. and Kent, J. H., *Seventeenth Symposium (International) on Combustion,* The Combustion Institute, Pittsburgh, PA, 1979, p. 279.

[75]Pope, S. B., "A Rotational Method of Determining Probability Distributions in Turbulent Reacting Flows," Imperical College, London, Dept. of Mechanical Engineering Rept. FS/77/19, 1977.

[76]Effelsberg, E. and Peters, N., *Combustion and Flame*, Vol. 50, 1983, p. 351.

[77]Pope, S. B., "Pdf Methods for Turbulent Reactive Flows," *Progress in Energy and Combustion Sciences,* Vol. 11, No. 2, 1985, p. 119.

[78]Kollmann, W. and Janicka, J., *The Physics of Fluids,* Vol. 25, 1982, p. 1755.

[79]Pope, S. B., *Combustion Science and Technology*, Vol. 25, 1981, p. 159.

[80]Mungal, M. G., Ph.D. Dissertation, California Institute of Technology, Pasadena, 1983.

[81]Mungal, M. G., Dimotakis, P. E., and Broadwell, J. E., AIAA Paper 83-0473, 1983.

[82]Dimotakis, P. E., "Entrainment and Growth of a Fully Developed Two-Dimensional Shear Layer," AIAA Paper 84-0368, 1984.

[83]Kerr, R., "Kolmogorov and Scalar Spectral Regimes in Numerical Turbulence," Paper AB8 presented at 36th Annual Meeting of Division of Fluid Dynamics, American Physical Society, Houston, 1983.

[84]Grötzbach, G., "Spatial Resolution Requirements for Direct Numerical Simulation of the Rayleigh-Benard Convection," *Journal of Computational Physics,* vol. 49, 1983, p. 241.

[85]Moin, P. and Kim, J., *Journal of Fluid Mechanics,* Vol. 118, 1982, p. 741.

[86]Kim, J., "The Effect of Rotation on Turbulence Structure," *Proceedings of 4th Symposium on Turbulent Shear Flows,* Springer-Verlag, Karlsruhe, FRG, Sept. 1983.

[87]Zalesak, S. T., *Journal of Computational Physics,* Vol. 31, 1979, p. 335.

[88]Ashurst, W. T., "Turbulent Flow Structure Effect on Diffusion and Premixed Flame Propagation," *Proceedings of Fourth GAMM Conference on Numerical Methods in Fluid Mechanics,* Oct. 1981, (also Sandia National Laboratories, Livermore, CA, Rept., SAND81-8785, Feb. 1982).

[89]Kerstein and Ashurst, W. T., "Lognormality of Gradients of Diffusive Scalars in Homogeneous, Two-Dimensional Mixing Systems," *The Physical of Fluids*, Vol. 27, 1984, p. 2819.

[90]Ashurst, W. T., Kerstein, A. R., Effelsberg, E., and Peters, N., "Calculated Scalar Dissipation in Two-Dimensional Flows," *Turbulent Shear Flows,* Vol. 4, edited by Bradbury et al., Springer-Verlag, New York, 1985 (also Sandia National Laboratories, Livermore, CA, Rept. SAND 82-8895A, 1982).

[91]Abdel-Gayed, R. G. and Bradley, D., "Dependence of Turbulent Burning Velocity on Turbulent Reynolds Number and Ratio of Laminar Burning Velocity to R.M.S. Turbulent Velocity," *Seventeenth Symposium (International) on Combustion,* The Combustion Institute, Pittsburgh, PA, 1978, pp. 1725-1735.

[92]Ashurst, W. T. and Barr, P. K., "Stochastic Calculation of Laminar Wrinkled Flame Propagation via Vortex Dynamics," *Combustion Science and Technology,* Vol. 34, 1983, p. 227.

[93]Dibble, R. W., Hartmann, V., Schefer, R. W., and Kollmann, W., "Conditional Sampling of Velocity and Scalars in Turbulent Flames Using Simultaneous LDV-Raman Scattering," Sandia National Laboratories, Livermore CA, Rept. SAND 84-8860, Nov. 1984; also, *Journal of Experiments in Fluids*, to be published.

[94]Dibble, R. W., Long, M. B., and Masri, A., "Observation of Local Flamelet Extinction in Turbulent Nonpremixed Jet Flames," submitted to *Combustion and Flame.*

[95]Namazian, M., Schefer, R. W., Long, M. B., Kelley, J., and Johnston, S. C., "$CH_4$ and CH Concentration Imaging in a Bluff-Body Stabilized Flame," submitted to the *Twenty-First Symposium (International) on Combustion.*